Perspective on the cosmic-ray electron spectrum above TeV

Kun Fang, Bing-Bing Wang, Xiao-Jun Bi, Su-Jie Lin, and Peng-Fei Yin

Key Laboratory of Particle Astrophysics, Institute of High Energy Physics,

Chinese Academy of Sciences, Beijing 100049, China

(Dated: December 1, 2016)

Abstract

The AMS-02 has measured the cosmic ray electron (plus positron) spectrum up to ∼TeV with an unprecedent precision. The spectrum can be well described by a power law without any obvious features above 10 GeV. The satellite instrument Dark Matter Particle Explorer (DAMPE), which was launched a year ago, will measure the electron spectrum up to 10 TeV with a high energy resolution. The cosmic electrons beyond TeV may be attributed to few local cosmic ray sources, such as supernova remnants. Therefore, spectral features, such as cutoff and bumps, can be expected at high energies. In this work we give a careful study on the perspective of the electron spectrum beyond TeV. We first examine our astrophysical source models on the latest leptonic data of AMS-02 to give a self-consistent picture. Then we focus on the discussion about the candidate sources which could be electron contributors above TeV. Depending on the properties of the local sources (especially on the nature of Vela), DAMPE may detect interesting features in the electron spectrum above TeV in the future.

I. INTRODUCTION

The Alpha Magnetic Spectrometer (AMS-02) launched in May 2011 has taken the measurement of cosmic ray (CR) leptonic spectra to a new level [1]. Unprecedentedly precise results have been released in the energy range from ~ 1 GeV to ~ 500 GeV for intensities of both electron and positron. The well-known electron/positron excess, which was uncovered by earlier satellite experiments such as the Payload for Antimatter Matter Exploration and Light-Nuclei Astrophysics (PAMELA) [2, 3] and the Fermi Large Area Telescope (Fermi-LAT) [4, 5], and also the anterior balloon-borne Advanced Thin Ionization Calorimeter (ATIC) experiment [6], has been confirmed by AMS-02. Sources which have the potential to provide primary electron/positron pairs, e.g., pulsars and annihilation of dark matter (DM), are thus involved into CR models to interpret those excesses. However, some global fittings of AMS-02 leptonic spectra indicate that the electron spectrum has a larger excess to the background than that of positron [7–9]. As the contributions of $e^{\pm}$ pairs from exotic sources like pulsars or DM are constrained by the positron spectrum, these sources seem not enough to explain the total electron excess.

A possible interpretation of the extra electron excess is the hardening in high energy range of the electron spectrum of the supernova remnant (SNR) background, which can be attributed to the fluctuation given by local discrete SNRs [9]. Thus the concept of dividing local SNRs and distant SNRs steps again into the spotlight. This concept was first put forward by Shen [10] and improved by later works. In the model of Atoyan *et al.* [11], a nearby (≤ 100 pc) and relatively young ($\leq 10^5$ yr) source and continuously distributed distant sources (≥ 1 kpc) contribute separately to the electron spectrum; they also adopted a energy dependent diffusion coefficient in the propagation model. Kobayashi *et al.* [12] went further on this scenario by using several real sources with known ages and distances as local electron accelerators. After the publishing of AMS-02 data, Di Mauro *et al.* [13] fit all the leptonic data simultaneously, applying the method similar to the works above when dealing with local and distant SNRs. They derived spectral index and normalization of injection spectrum of individual SNR from radio observations, comparing with uniform injection spectral parameters of all the sources adopted in Ref. [12].

In fact, there are alternative explanations toward the electron/positron excess, such as improper propagation parameters used in previous works [14]. In these cases, exceptional

consideration of local sources may not be necessary to keep consistency with the AMS-02 data. However, the ground-based Cherenkov telescopes like the High Energy Stereoscopic System (HESS) [15, 16] and the Very Energetic Radiation Imaging Telescope Array System (VERITAS) [17] seemed to detect a cut-off around ~ 1 TeV in the $e^- + e^+$ spectrum, which cannot be described by a continuous distributed background. The Dark Matter Particle Explorer (DAMPE) [18] launched in December 2015 aims to measure electrons in the range of 5 GeV$-$10 TeV with unprecedented energy resolution (1.5% at 100 GeV). As nearby sources have the potential to contribute to the highest energy range covered by DAMPE, we can expect to see some spectral features in future DAMPE results. In this case, separating local sources from the continuous distribution would be inevitable.

Basing on previous works mentioned above, we perform a careful analysis of the local SNRs and their parameters of injection spectra. We assume that pulsars are extra positron sources, and perform global fittings to the latest leptonic data of AMS-02 for several SNR parameter settings. We show below that the choice of parameters of a particular SNR has a significant influence on its contribution. Although the electron energy range covered by AMS-02 is under TeV, fittings to the AMS-02 leptonic data provide a self-consistent picture for the astrophysical source models. As the local sources accounting for the AMS-02 results may provide contribution to the TeV scale, the AMS-02 data could also constrain the properties of the predicted $e^- + e^+$ spectrum above $\sim$ TeV. Combining with the fitting results, we then discuss the parameters of the local sources which have the potential to contribute to TeV and give further predictions of the $e^- + e^+$ spectrum up to the energy range of 10 TeV, which can be measured by DAMPE.

This paper is organized as follows. In Sec. II, we describe our calculation towards the injection and propagation of Galactic electrons and positrons to get leptonic spectra. The results of global fittings to leptonic data of AMS-02 and our further predictions to the electron spectrum in the TeV range are presented in Sec. III and Sec. IV, respectively. We summarize our work in the last section.

II. METHOD

In this section, we introduce the semi-analytical solution to the propagation equation in the first part. Then we discuss the possibly that SNRs are the most important sources of

high energy CR electrons. Discussions of other sources, including pulsars and secondary electrons/positrons, are given in the later subsections.

A. Propagation of Cosmic Rays

The propagation of CR electrons in the Galaxy can be described by the diffusion equation with additional consideration of energy loss during their journey, which may be written as

$$\frac{dN}{dt} - \nabla(D\nabla N) - \frac{\partial}{\partial E}(bE) = Q\,, \tag{1}$$

where N is the number density of particles, D denotes the diffusion coefficient, b denotes the energy-loss rate and Q is the CR source function. Galactic convection and diffusive reacceleration are not taken into account here, since they have little effect above 10 GeV [19]. We treat the propagation zone of CRs as a cylindrical slab, with radius of 20 kpc [19] and a half thickness z_h. The diffusion coefficient D depends on the energy of CRs, which has the form $D(E) = \beta D_0 (R/1\,\mathrm{GV})^\delta$, where D_0 and δ are both constants, β is the velocity of particles in the unit of light speed and R is the rigidity of CRs. To give a constraint of major propagation parameters—(D_0,δ,z_h), Boron-to-Carbon ratio (B/C) is widely used. Unstable-to-stable beryllium (^{10}Be/^{9}Be) is also helpful to constrain CR propagation. We adopt the B/C data of ACE [20], AMS-02 [21], ^{10}Be/^{9}Be data of Ulysses [22], ACE [23], Voyager [24], IMP [25], ISEE-3 [25], ISOMAX [26], and embed the CR propagation code in the Markov Chain Monte Carlo (MCMC) sampler to acquire best fitted propagation parameters (this work is in preparation). We adopt $D_0 = 2.12 \times 10^{28}\,\mathrm{cm^2 s^{-1}}$, $\delta = 0.548$, $z_h = 3.8$ kpc in this work.

Positrons and electrons with energy higher than 10 GeV suffer from energy loss during their propagation mainly by synchrotron radiation in the Galactic magnetic field and inverse Compton radiation in the interstellar radiation field consisting of stellar radiation, reemited infrared radiation from dust, and cosmic microwave background (CMB). We set the interstellar magnetic field in the Galaxy to be 1 μG to get the synchrotron term [19]. For the inverse Compton process, if we use the cross section for Thomson scattering, the energy-loss rate $b(E)$ has a quadratic dependence on energy:
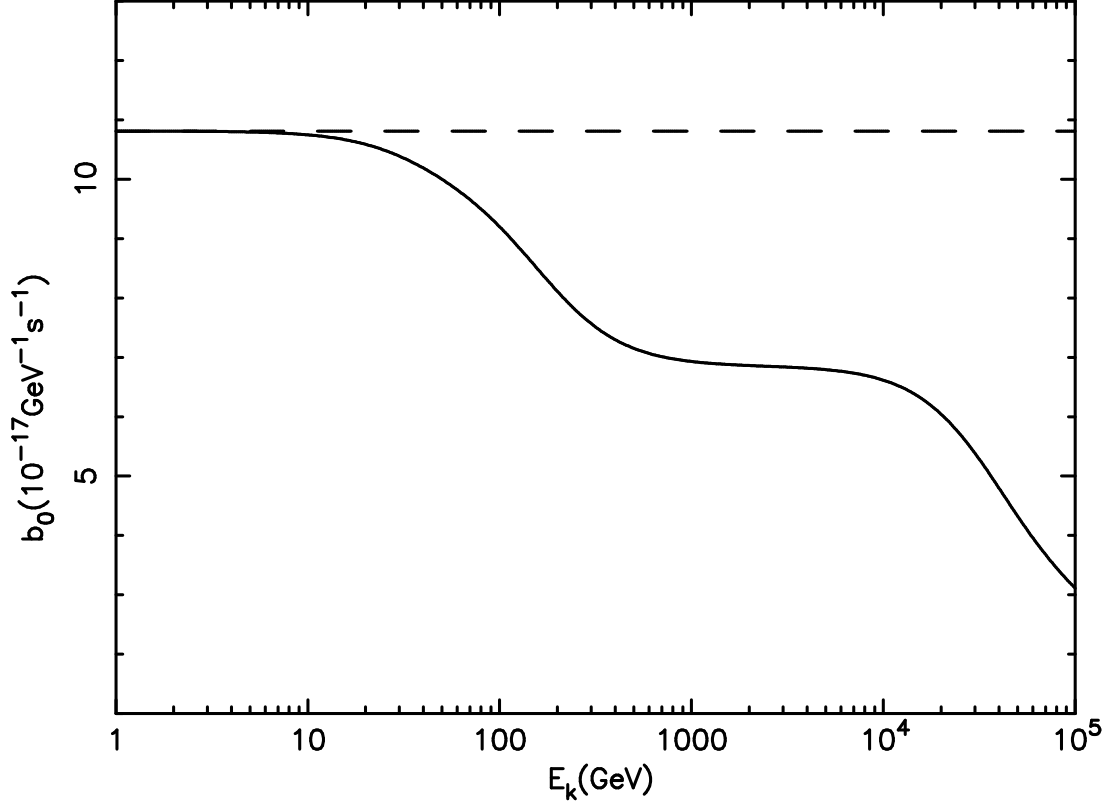
$$\frac{dE}{dt} = -b_0 E^2\,, \tag{2}$$

4

FIG. 1. Energy-loss coefficient b_0 as a function of $e^{\pm}$ energy. The dashed line stands for the case of Thomson approximation and the solid line describes the drops of b_0 due to Klein-Nishina correction.

where b_0 is a constant. However, when the energy comes higher, a relativistic correction to the cross section, namely a Klein-Nishina cross section, is needed. Here we adopt the description of Ref. [27] which gives a reconcilable approximation between Thomson limit and Klein-Nishina limit. The temperature and energy density of radiation field components are: 20000 K and $0.09\,\mathrm{eV\,cm^{-3}}$ for type B stars, 5000 K and $0.3\,\mathrm{eV\,cm^{-3}}$ for type G-K stars, 20 K and $0.4\,\mathrm{eV\,cm^{-3}}$ for infrared dust, and 2.7 K and $0.25\,\mathrm{eV\,cm^{-3}}$ for CMB. In this case, b_0 is not a constant anymore but decreases with the energy as shown in Fig. 1. We can find from Fig. 1 that the relativistic correction becomes important as long as energies of electrons/positrons are higher than 10 GeV. We still use the symbol b_0, which has the connotation of $b_0(E)$, in our later work for convenience.

Cylindrical coordinate is applied in our work to describe the disc-like geometry of the propagation zone, and the location of the Earth is set to be zero. For a point source with

burst-like injection, the source function can be written as

$$Q(E, t, r, z) = Q(E)\delta(t - t_s)\delta(r - r_s)\delta(z - z_s) \,, \tag{3}$$

where $Q(E)$ represents the energy distribution of injection, t_s is the time of CR injection, r_s and z_s are radial and verticle location of the source, respectively. As long as Galactic CR sources are mostly distributed in a much thinner vertical scale comparing with z_h and so does the solar system, we assume $z_s = 0$ in our work for all the sources. Then the time-dependent Eq.(1) can be solved semi-analytically with the help of Green's function $G(E, t, r \leftarrow E_s, t_s, r_s)$ working in the Fourier space. We follow the Green's function used in Ref. [12]:

$$\begin{aligned}
G(E, t, r \leftarrow E_s, t_s, r_s) = {}& \delta(E_s - E_0)\frac{b(E_0)}{b(E)}\frac{1}{\pi\lambda^2}\exp\left[-\frac{(r - r_s)^2}{\lambda^2}\right] \\
& \times \sum_{n=0}^{\infty}\frac{1}{z_h}\exp\left(-\frac{\lambda^2 k_n^2}{4}\right) \,,
\end{aligned} \tag{4}$$

where $k_n = (2n + 1)\pi/(2z_h)$, $E_0 = E/[1 - b_0 E(t - t_s)]$, and

$$\lambda \equiv 2\left(\int_E^{E_0}\frac{D(E')dE'}{b(E')}\right)^{1/2} \tag{5}$$

is the diffusion distance for particles with initial energy E_0 and final energy E. The solution of Eq. (1) has the form of $G(E, t, r \leftarrow E_s, t_s, r_s)Q(E_s, t_s, r_s)$, so the observed CRs contributed by a source with distance r and age t should be expressed as

$$\begin{aligned}
N(E, t, r) = {}& \frac{1}{\pi\lambda^2}(1 - b_0 Et)^{-2}\exp\left(-\frac{r^2}{\lambda^2}\right)Q\left(\frac{E}{1 - b_0 Et}\right) \\
& \times \sum_{n=0}^{\infty}\frac{1}{z_h}\exp\left(-\frac{\lambda^2 k_n^2}{4}\right) \,.
\end{aligned} \tag{6}$$

However, considering the efficiency of doing numerical calculation, Eq. (6) may not be a good expression since we need to include more terms in higher energy range to guarantee precision of the calculation. Thus a spherically symmetric time-dependent solution to Eq. (1), which has a form of [28, 29]

$$N(E, t, r) = \frac{1}{(\pi\lambda^2)^{3/2}}(1 - b_0 Et)^{-2}\exp\left(-\frac{r^2}{\lambda^2}\right)Q\left(\frac{E}{1 - b_0 Et}\right) \,, \tag{7}$$

can be treated as a substitute of Eq. (6). Given the disc-like geometry of propagation zone, Eq. (7) is valid when $\lambda \ll z_h$. Assuming E is close enough to E_0, the diffusion distance
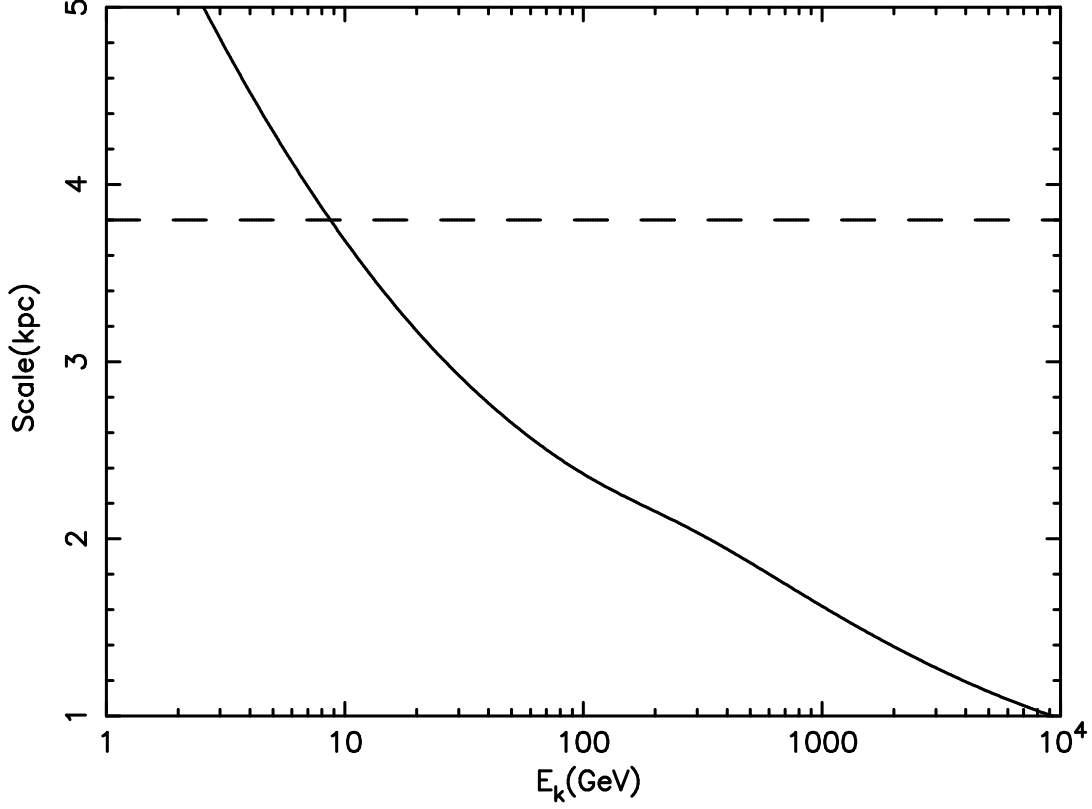
FIG. 2. Comparision between diffusion distance of CRs and half-thickness of propagation zone. The solid line represents the diffusion scale $\lambda \sim 2\sqrt{D(E)t}$ while the dashed line marks z_h.

defined in Eq. (5) can be approximated by $2\sqrt{D(E)t}$. As shown in Fig. 2, the condition $\lambda < z_h$ is always satisfied as long as $E > 10\,\text{GeV}$, and the difference increases in higher energy. In fact, we find the error is less than 1% for $E > 10\,\text{GeV}$ after calculating ratios between these two expressions.

B. SNRs as Electron Source

1. Local SNRs and SNR Background

SNRs are believed to be the main astrophysical sources of primary Galactic CRs, such as nucleus and electrons. Particles can be boosted to very high energy through diffusive shock wave acceleration in SNR. However, among the accelerated particles, electrons/positrons undergo significant energy loss during their propagation through electromagnetic radiation. Eq. (2) indicates the life time of an electron is roughly $1/(b_0 E)$, thus electrons with higher energy become inactive faster. Since $\delta < 1$, the diffusion distance $2\sqrt{D(E)t}$ has an inverse

7

relationship with electron energy. For example, electrons in $\sim$ TeV fade within a radius of roughly 1 kpc from their source. Thus high energy part of electron spectrum can only be contributed by several local sources, and a simple continuous source distribution is no longer valid due to the spectral fluctuations induced by those few sources. Then it is important to separate local discrete sources from distant sources in calculation, as first proposed by Shen [10]. We treat SNRs within 1 kpc as local sources and farther sources as background contributors of electrons [12]. The intensity of electrons from a SNR nearby can be simply expressed by

$$I(E) = \frac{c}{4\pi} N(E, t, r) \,. \tag{8}$$

In order to obtain distant components, we calculate the electron spectrum produced by a smooth distribution of SNRs in whole range of distance and age first, and then subtract the local components in continuous form. We set supernova explosion rate to be $f = 4$ century^{-1} galaxy^{-1} [19]. Since about 2/3 of supernovae are expected to be type II supernova, we can use the population of pulsars to describe the spatial distribution of SNRs. Here we choose the Galactic distribution of pulsars given by Ref. [30] as

$$\rho(R) \sim R^n \exp\left(-\frac{R}{\sigma}\right) \,, \tag{9}$$

where $n = 2.35, \sigma = 1.528$ kpc and R is the distance to the Galactic center. Note that the zero point of this distribution is the Galactic center, rather than the solar system used in our work. Thus ρ should also depend on the azimuth angle φ. Here we aim to find how local sources create spectrum features in TeV range. As the diffusion distance of 1 kpc corresponds to a electron cooling time of roughly 3×10^5 yr, sources older than this age are treated as background SNRs in our calculation. Finally we get the electron spectrum of background component:

$$I(E) = \frac{c}{4\pi} \left(\int_0^{\frac{1}{b_0 E}} dt \int_0^\infty dr \int_0^{2\pi} d\varphi - \int_0^{t_m} dt \int_0^{r_m} dr \int_0^{2\pi} d\varphi \right) \tag{10}$$
$$\times f \, \rho(r, \varphi) \, N(E, t, r) \, r \,,$$

where $\rho(r, \varphi)$ is the normalized distribution, $r_m = 1$ kpc and $t_m = 3 \times 10^5$ yr for the case $1/(b_0 E) > 3 \times 10^5$ yr (otherwise t_m takes $1/(b_0 E)$). Indeed, full propagation equation with consideration of convection and reacceleration may be solved with public numerical tool GALPROP [31] which can give a more accurate result. Nevertheless, the spatial zero point

8

Source	Other Name	B_r^{1GHz}[Jy]	α_r	Size[arcmin]	r[kpc]	t[kyr]	Ref.
G065.3+05.7	-	52	0.58	310×240	0.9	26	[32–35]
G074.0–08.5	Cygnus Loop	175	0.4	230×160	0.54	10	[32, 36, 37]
G114.3+00.3	-	6.4	0.49	90×55	0.7	7.7	[32, 38–40]
G127.1+00.5	R5	12	0.43	45	1	[20, 30]	[32, 38, 39, 41, 42]
G156.2+05.7	-	5	0.53	110	1.0	[15, 26]	[32, 39, 43–46]
G160.9+02.6	HB9	88	0.59	140×120	0.8	[4, 7]	[32, 38, 39, 47, 48]
G203.0+12.0	Monogem Ring	-	-	-	0.3	86	[49, 50]
G263.9–03.3	Vela YZ	varies	varies	255	0.29	11.3	[32, 51–54]
G266.2–01.2	Vela Jr.	50	0.3	120	0.75	[1.7, 4.3]	[32, 55–58]
G328.3+17.6	Loop I (NPS)	-	-	-	0.1	200	[59, 60]
G347.3–00.5	RXJ1713.7-3946	4	0.3	65×55	1	1.6	[32, 61, 62]

TABLE I. Basic parameters for local SNRs within 1 kpc. The columns show the Green catalog name, the association name, the radio flux B_r^{1GHz}, the radio spectrum index α_r, the distance r and the SNR age t. Note that t is the observed age, the actual age should be $T = t + r/c$.

used in GALPROP is the center of the Galaxy, we may need to do some troublesome work to divide local sources from the background. That's the reason we choose an semi-analytic treatment toward Eq. (1).

2. Parameters of SNRs

For SNRs, particles are accelerated by shock acceleration mechanism, or say, the first order Fermi acceleration. The energy spectrum produced by Fermi acceleration is thought to be a power law form. Taking energy loss and escape of particles into account, the emergent spectrum of SNR can be described by a power law form with an exponential cutoff:

$$Q(E) = Q_0(E/1\,\mathrm{GeV})^{-\gamma}\exp(-E/E_c)\,, \tag{11}$$

where Q_0 is the normalization of the injection spectrum. Note that distant SNRs are treated as a continuous distribution. Thus we assume that they share common Q_0 and γ, and set these two parameters to be free in following fittings. The energy cut-off is fixed at 20 TeV for

background sources. For local SNRs, we attempt to investigate their parameters individually. Table I lists objects locating within 1 kpc included by the Green catalog of SNRs [32] (of course those with a measured distance) with two additional sources Monogem Ring and Loop I.

Several SNRs have gone through multi-wavelength measurements, from radio to γ-ray bands, which are helpful to estimate parameters in Eq. (11). These sources include HB9 (radio and γ-ray), Vela Jr. (radio, X-ray and γ-ray), RX J1713.7-3496 (radio, X-ray and γ-ray), and Cygnus loop (radio and γ-ray). Note that we just pick observations with available data. Radio and X-ray emissions are produced by the synchrotron radiation of relativistic electrons accelerated in the SNR, while γ-ray emissions could have either a leptonic origin or a hadronic origin, which are generated through scattering of background photons by relativistic electrons or through π^0 decay resulting from the collision of accelerated protons with ions in the background plasma. As we are interested in the electron spectrum, a purely leptonic model is the priority in our fitting. If the leptonic fitting fails, this model is replaced by a hybrid model, where contributions from electrons and protons are comparable in γ-ray spectrum. Purely hadronic model would not be discussed in our work.

For the leptonic model, the energy spectrum of accelerated electrons still has the form of Eq. (11), while we remark the parameters in those expression as $Q_{0,e}$, γ_e and $E_{c,e}$, to distinguish from the case of proton. The background radiation fields consist of interstellar infrared radiation, optical radiation and CMB. The contributions to the inverse Compton γ-ray spectrum from the interstellar radiation field (ISRF) are more important than that from CMB [63]. Here we adopt the ISRF model given by Ref. [64]. In the hybrid model, the energy spectrum of protons has the same form as that of electrons, where $Q_{0,p}$, γ_p and $E_{c,p}$ are corresponding normalization parameter, spectral index and cut-off energy of protons. Assuming charged particles share the same acceleration mechanism, the spectral index of protons could be identical to that of electrons [63, 65]. Thus the four free parameters in leptonic model are $Q_{0,e}$, γ_e, $E_{c,e}$ and magnetic field B. For the case of hybrid model, there are three additional parameters, $Q_{0,p}$, $E_{c,p}$ and number density of target proton N_{H}.

We apply naima, a python-based package, for computing non-thermal radiation processes and fitting the spectral energy distributions [66]. It uses Markov-Chain Monte Carlo emcee sampling [67] to find best-fit parameters of physical radiation models and thus determines the radiation mechanism behind the observed emission. The parameters of the best-fit
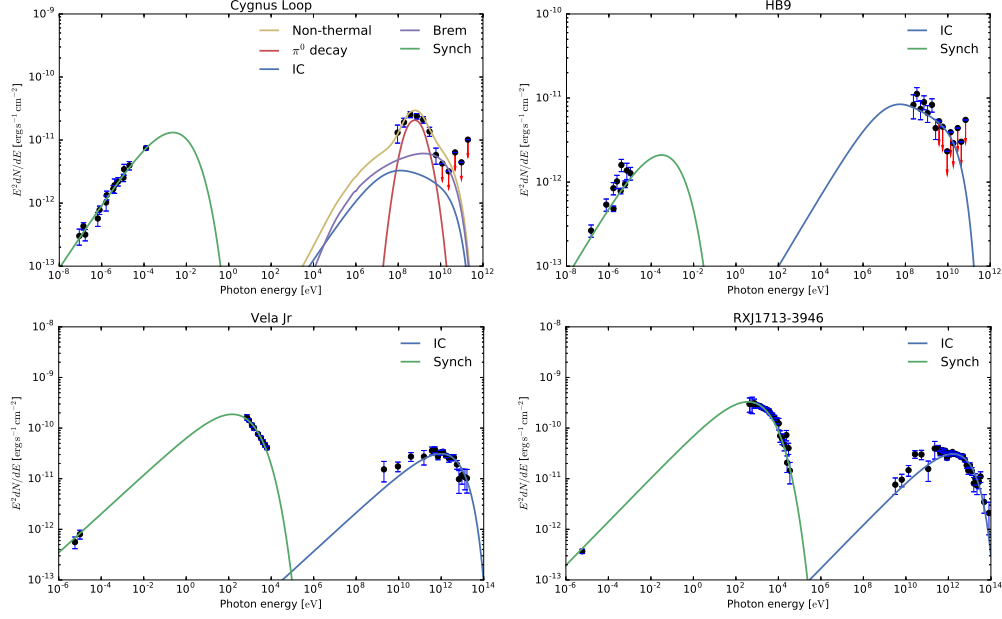
FIG. 3. Energy spectrum distribution of the sources Cygnus Loop, HB9, Vela Jr. and RX J1713.7-3946. The components are: synchrotron (green line), IC(blue line), non-thermal bremsstrahlung (purple line), neutral pion decay (red line). Total γ-ray emission for hybrid scenario is marked by yellow line. References for the fitted data points are given in Table II.

models are compiled in Table II and the best-fit spectra are shown in Fig. 3.

Different from four SNRs mentioned above, we need other approaches to determine parameters for other SNRs without precise high energy γ-ray observations. Assuming the radio emissions of SNRs are entirely induced by synchrotron emissions of electrons, Di Mauro $et\ al.$ [13] provided an estimation method of Q_0 as

$$Q_0 = 1.2 \times 10^{47} \text{ GeV}^{-1} (0.79)^\gamma \left(\frac{r}{\text{kpc}} \right)^2 \left(\frac{B}{100\mu\text{G}} \right)^{-(\gamma+1)/2} \left(\frac{B_r^{1\text{GHz}}}{\text{Jy}} \right) , \qquad (12)$$

which relies on spectral index γ, source distance r, magnetic field B in SNR and the radio flux at 1 GHz $B_r^{1\text{GHz}}$. For the synchrotron emission of electron system, the electron spectral index can be derived from the photon spectral index. Thus we have $\gamma = 2\alpha_r + 1$, where α_r is the radio spectral index. We list $B_r^{1\text{GHz}}$ and α_r in Table I. Another critical parameter B can only be approximately estimated by several methods, such as Zeeman effect, Faraday rotation, and minimum energy or equipartition. The equipartition or minimum energy method calculates magnetic field only depending on the radio synchrotron emission of source [68]. It is a useful tool if no other data of the source is available. According to the result of

11

Arbutina *et al.* [69], we can obtain the magnetic field of SNR as

$$
\begin{aligned}
B[\text{G}] \approx & \left[6.286 \times 10^{(9\gamma-79)/2} \frac{\gamma+1}{\gamma-1} \frac{\Gamma(\frac{3-\gamma}{2})\Gamma(\frac{\gamma-2}{2})\Gamma(\frac{\gamma+7}{4})}{\Gamma(\frac{\gamma+5}{4})} (m_e c^2)^{2-\gamma} \right. \\
& \left. \times \frac{(2c_1)^{(1-\gamma)/2}}{c_5} (1+\kappa) \frac{B_r^{1\text{GHz}}[\text{Jy}]}{f \, r[\text{kpc}] \, \theta[\text{arcmin}]^3} \right]^{2/(\gamma+5)} ,
\end{aligned} \tag{13}
$$

where $m_e c^2$ is rest energy of electron, c_1 and $c_5 = c_3 \Gamma(\frac{3\gamma-1}{12})\Gamma(\frac{3\gamma+19}{12})/(\gamma+1)$ are defined in Ref. [70], f is the volume filling factor of radio emission, θ is the angular radius of SNR which can be found in Green catalog. In Eq. (13), κ is a parameter depending on γ and ion abundances of SNR. We adopt a typical value $f = 0.25$ and simple ISM abundance H:He=10:1 in our estimation. Note that this minimum energy method is applicable only for mature SNRs with $\alpha > 0.5$. For G114.3+00.3 and G127.1+00.5, we take a typical value of $B = 30 \, \mu\text{G}$. Finally, We follow the method proposed by Yamazaki *et al.* [71] to give an estimation to E_c. When the age of a SNR meets $t \gtrsim 10^3$ yr, synchrotron loss restricts the maximum energy of electrons. Thus we have

$$
E_c = 14 \, \text{TeV} \, h^{-1/2} \, v_{s,8} \, (B/10\mu\text{G})^{-1/2} , \tag{14}
$$

where $v_{s,8}$ is the shock velocity in unit of $10^8 \, \text{cm s}^{-1}$ which depends on evolution of SNR. See details in Ref. [71] for the definition of h and here we take it to be unit.

So far we have estimated parameters for all the sources in Table I except for Vela(XYZ), Monogem Ring and Loop I. The results are listed in Table II. Vela(XYZ) is generally believed to be an important local source of CRs. We discuss it in detail in the next section. For Monogem ring and Loop I, they are classified as possible or probable SNRs by Green [32] and are not included in the catalog due to the lack of understanding to them. We treat them as potential sources of electrons in the next section and set their parameters to be free. Note that all those estimations of SNR parameters rely on the electromagnetic radiations of SNR. These emissions are not produced by electrons observed today but some 'younger' ones in SNRs. This implies that even if observations of photon emission are precise enough, the derived electron parameters may be different from those of injected electrons due to the variation of parameters along with the evolution of SNRs. Therefore the aim of our estimation is to give some reference values for electron injection parameters, but far from to 'determine' them.

Source	$B[\mu\text{G}]$	$Q_{0,e}[10^{49}\text{GeV}^{-1}]$	γ_e	$E_{c,e}[\text{TeV}]$	$W_e[10^{48}\text{erg}]$	Ref.
G065.3+05.7	10.6	10.5	2.16	7.2	0.77	-
G074.0–08.5	9.7	10	1.99	0.072	0.63	[72–74]
G114.3+00.3	30	0.14	1.98	9.3	0.02	-
G127.1+00.5	30	0.52	1.86	4.6	0.12	-
G156.2+05.7	13	0.83	2.06	8.4	0.09	-
G160.9+02.6	2.3	130	2.15	0.065	5.66	[47, 48, 75, 76]
G266.2–01.2	8.9	9.6	2.23	25.4	0.59	[77–79]
G347.3–00.5	11.9	5.7	2.14	31	0.48	[80–84]

TABLE II. The electron spectrum parameters for our sample. The parameters of HB9, Vela Jr. and RXJ1713.7-3946 are obtained by fitting the multi-wavelength emission by leptonic model. The hybrid model give better fitting for Cygnus loop, and the extra parameter are $Q_{0,p} = 1.5 \times 10^{52}\,\text{GeV}^{-1}$, $E_{c,p} = 12\,\text{GeV}$, $N_H = 0.46\,\text{cm}^{-3}$. Magnetic field strength of G065.3+05.7 and G156.2+05.7 are deduced from Eq. (13), and we adopt 30 μG for G114.3+00.3 and G127.1+00.5. For those sources $Q_{0,e}$ and $E_{c,e}$ are derived from Eq. (12) and Eq. (14) respectively, while γ_e is given by the relation $\gamma = 2\alpha_r + 1$. References for the multi-wavelength fitting data are given in the last column.

C. PWN as Electron and Positron Source

Pulsars are known to be the most important astrophysical sources of high energy electron/positron pairs in the Galaxy [85]. They produce relativistic wind carrying charged particles at the cost of their spin-down energy [86]. Since pulsar is formed in SN explosion, it is initially surrounded by its companion SNR. When the relativistic pulsar wind impacts on the cold SN ejecta which expands with a slower velocity, a termination shock is formed besides a forward shock. The termination shock propagates inward and reaches the radius where the outward pressure of pulsar wind balances the internal pressure of the shocked bubble (see Ref. [87] and references therein). The shocked region is dubbed the pulsar wind nebula (PWN). After particles inter the PWN, they are confined by the magnetic field here for a long period, until the crushing of the PWN. Thus the spectrum of electrons and positrons injected into ISM should be the spectrum inside the PWN when it is disrupted, other than the spectrum inside the magnetosphere of pulsar [29]. Like SNRs, pulsars can be

13

divided into local pulsars and smooth distant components. Delahaye *et al.* [19] find that the contribution from pulsar background is negligible compared to those from local ones, thus we do not take the former into account in our calculation. Parameters of nearby pulsars can be found in the ATNF catalog [88].

We assume the injection $e^\pm$ spectra of PWNs have the same form of Eq. (11); a burst-like injection spectrum is also adopted. Note that the spectral index used here is associated with the PWN, and cannot be derived from the spectral index of the pulsed radio emission from pulsar given in the ATNF catalog. Thus if the radio spectral index of PWN is not available, we set $\gamma_{\rm PWN}$ as a free parameter in the following fittings. The normalization parameter Q_0 is linked to the spin-down energy W_p dissipated by pulsar by:

$$\int_{E_{\rm min}}^{\infty} Q(E)E\,dE = \eta W_p\,, \tag{15}$$

where $E_{\rm min} = 0.1\,{\rm GeV}$ and η is the efficiency of energy conversion treated as another free parameter. The spin-down luminosity $\dot{E}$ evolves with the age of pulsar t as $\dot{E} = \dot{E}_0(1 + t/\tau_0)^{-2}$ [89], where $\dot{E}_0$ is the initial spin-down luminosity, τ_0 is the spin-down time scale of the pulsar, assumed to be 10 kyr in our work. Integrating $\dot{E}$ with time, we get the expression of spin-down energy $W_p = \dot{E}\,t\,(1 + t/\tau_0)$, where $\dot{E}$ and t can be found in ATNF catalog. For the cut-off energy, We take $E_c = 2\,{\rm TeV}$ following the work of Ref. [13].

D. Secondary Electrons and Positrons

Secondary electrons and positrons are created by inelastic collision between CR nuclei and ISM. The CR nuclei mainly consist of protons and α particles while H and He are major components of ISM. As can be seen from the AMS-02 result, the positron fraction is smaller than 10% below $\sim 100\,{\rm GeV}$, where secondary positrons should contribute less than 10%. Since the spallation process produces more positrons than electrons, secondary electrons possess a further smaller percentage comparing to the total electron intensity in the range mentioned above. Thus we neglect the secondary electron component and concentrate on secondary positrons. In this part, our calculation follows the method of Ref. [90]. The source function of secondary e^+ is assumed to be steady and homogeneous in a slab geometry:

$$Q_{sec}(E) = 4\pi \sum_{i,j} n_j \int dE'\, \Phi_i(E') \frac{d\sigma_{ij}(E', E)}{dE} \tag{16}$$

14

so that the propagation equation can be solved semi-analytically with a relatively simple form (see [90] for details). In Eq. (16), i and j mark the species of CR nuclei and ISM gas respectively. The number density of ISM is set to be $n_{\mathrm{H}} = 0.9\,\mathrm{cm}^{-3}$ and $n_{\mathrm{He}} = 0.1\,\mathrm{cm}^{-3}$. The intensities of incident CR nuclei are donated by Φ which can be estimated by the observed intensities at earth. We employ the expression of Φ proposed by Shikaze *et al.* [91]. Di Mauro *et al.* [13] fit the AMS-02 data of proton and Helium to refresh the parameters in the model of Φ. For differential scattering cross-section $d\sigma/dE$, Kamae *et al.* [92] provides functional formulae for proton-proton collision. Empirical rescaling based on this result are applied to estimate cross-section of collision between other species [93]. Besides, we introduce a free parameter c_{e+} to rescale the secondary intensity, considering the uncertainty in the calculation above, to accommodate the data.

III.   FITTING TO THE AMS-02 DATA

Up to now, AMS-02 provides the most precise measurement of leptonic spectra below 1 TeV. We attempt to perform global fittings to all the leptonic data released by the AMS-02 Collaboration, including the positron fraction, positron plus electron spectrum, positron spectrum and electron spectrum [94–96]. The global fitting is useful to set stringent constraints for astrophysical contributors, and leads to a self-consistent picture [97].

Astrophysical components considered in our model have been discussed in the previous section, including background SNRs as main contributors of electrons in low energy range, local SNRs as dominant contributors of electrons in higher energy range, secondary positrons which dominate low energy part of positron spectrum, and local PWNs as predominant components in higher energy range of positrons.

In this section, we explain the AMS-02 data by using several astrophysical source models. The characteristic of each model depends on which sources are chosen to be predominant local SNRs. We can see below that according to the calculation in the previous section, local SNRs listed in Table II hardly have significant contributions to electron intensity within the energy range of AMS-02. They would not play the role of predominant local sources in this section; we simply add their contributions for each model.

Positrons contribute only $\sim 10\%$ of the total $e^- + e^+$ intensity. We would like to simplify the constitution of positron spectrum, and use a single PWN to fit the high energy part of

e^+ spectrum. Di Mauro *et al.* [13] have already given a 'single-source' analysis in their work and find that Geminga is the most proper one among their candidates. However, due to the old age of Geminga (342 kyr), a spectral roll-off may appear below 1 TeV. Thus if Geminga is chosen as the single PWN, it may induce a slight break in $e^- + e^+$ spectrum below 1 TeV.

Another famous pulsar B0656+14, also namely Monogem, is believed to be associated with Monogem Ring. It lies at a distance of 0.28 kpc with an age of 112 kyr which is younger than Geminga [88]. Monogem has the potential to significantly contribute to the positron spectrum from 100 GeV to 1 TeV (see Table 4 of Ref. [19]). Also, we can see from Figure 2 of Ref. [13], the spectrum of Monogem has a similar shape with that of total PWNs in the ATNF catalog. Therefore we expect a PWN with the similar distance and age as Monogem can play a role as the single positron source.

We would show in following subsections that Monogem does well in the fittings as a single positron source. Comparing with the total spin-down energy of Geminga 1.26×10^{49} erg and the required η of only 0.27 in the 'single source' model in Ref. [13], the fittings for Monogem requires a large η (0.6~0.8 in our models) due to its low spin-down energy of 1.78×10^{48} erg. However, Monogem can extent its electron/positron spectra to higher energies than Geminga because of its smaller lifetime, and is helpful to explain the cut-off indicated by HESS and VERITAS data. In this work, we take Monogem as the single positron source in our fittings.

Hence, for different models shown below, the common free parameters are Q_0 and γ for SNR background, rescaling parameter c_{e+} for secondary positron, η and γ_{PWN} for Monogem and a solar modulation potential ϕ to accommodate data below tens of GeV.

A. Vela YZ

It is widely believed that the famous and well studied SNR Vela is an important local source of Galactic CRs due to its appropriate age and distance and its strong radio emission [12, 13]. Fig. 4 shows the contours of electron intensity as a function of r and t of source at different energy, assuming typical input energy (10^{48} erg), spectral index (2.0) and cut-off energy (10 TeV) of electrons. Every source in Table I is marked in Fig. 4. It is clearly that Vela predominates over other local SNRs above hundreds of GeV, and this is where the observed electron excess to continuous SNR model appears.

Vela shows a shell-like radio structure consisting of three principle regions, dubbed Vela X,
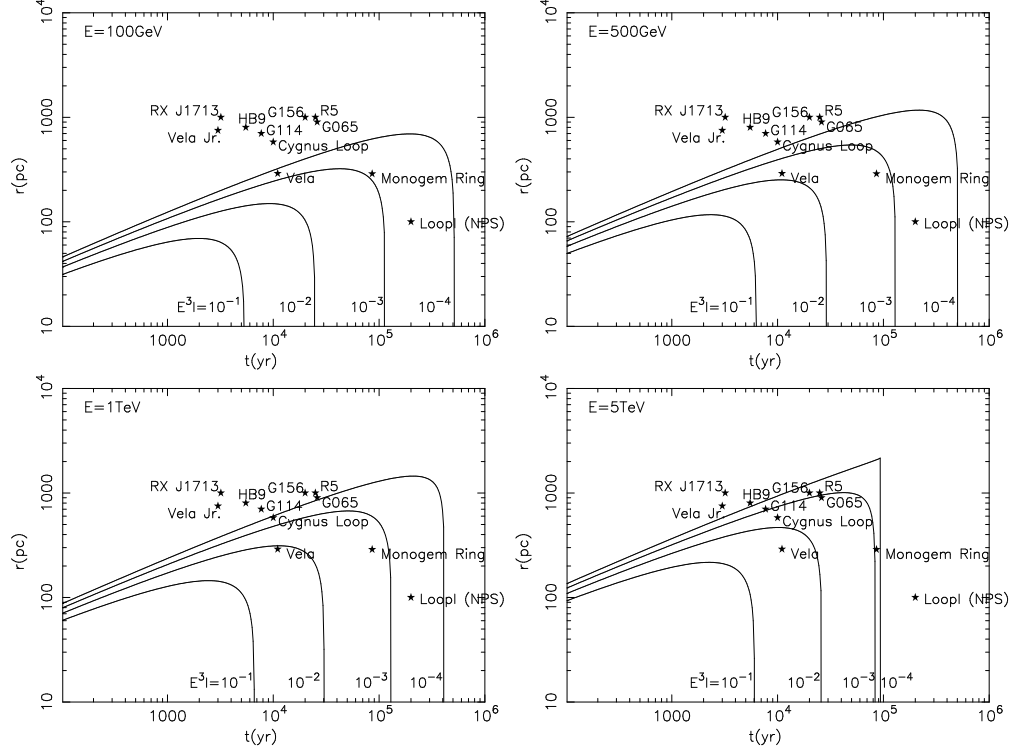
FIG. 4. Contours of electron intensity as a function of ages and distances of local SNRs. Top left: $E = 100\,\mathrm{GeV}$; top right: $E = 500\,\mathrm{GeV}$; bottom left: $E = 1\,\mathrm{TeV}$; bottom right: $E = 5\,\mathrm{TeV}$. Contour lines in each graph represent for $E^3 I(E) = 10^{-1}$, 10^{-2}, 10^{-3}, $10^{-4}\,\mathrm{GeV^2\,cm^{-2}\,s^{-1}\,sr^{-1}}$, as noted in each graph. In the calculation, the spectral index, cut-off energy and total input energy of electrons are assumed to be 2.0, 10 TeV and 10^{48} erg, respectively. Sources listed in Table I are also marked in each graph. Since every SNR is constrained to share the same injection spectrum here, this figure is for reference only.

Y and Z [98]. A weaker component Vela W observed by Alvarez *et al.* [51] is not considered in our work. Milne [99] find the spectrum of Vela X was remarkably flat than that of Vela Y and Z. This unusual spectrum was first explained by Weiler and Panagia [100]. They argued that Vela X should belong to plerions and PWNs like Crab, rather than shell-type SNRs like its siblings Vela Y and Z. This point of view has been accepted in later works. Consequently, when we estimate the contribution from Vela SNR, we ought to divide Vela X from Vela YZ. PWNs have different mechanisms of acceleration and evolution from shell-type SNRs. This means that they cannot share parameters, such as spectral index or cut-off energy, with the later.

In the first model, we set Vela YZ as the unique predominant SNR and aim to check

17

if it can give a good interpretation to AMS-02 data. As suggested by Ref. [13], we fix the magnetic field to be 30 μG and cut-off energy to be 2 TeV. In the Green catalog of SNRs, the radio spectral index of Vela is denoted as 'varies' perhaps due to the discrepancy between Vela X and YZ. We put spectral index α_{vela} of Vela YZ into the group of free parameters in this model. A free α_{vela} leads to the uncertainty of $B_r^{1\text{GHz}}$. The radio flux of Vela YZ at 960 MHz is measured to be 1100 Jy [51], so we set $B_r^{1\text{GHz}} = 1000$ Jy here as an estimation. We seek the best-fit model by minimizing chi-squared statics between model and data points. The result of global fitting to AMS-02 data are shown in Fig. 5. In each sub-graph, all the components are drawn to show their contribution and black solid line represents the fitting result. The best-fit reduced χ^2 is 0.473 for 182 degrees of freedom (d.o.f.), while the best-fit parameters are compiled in Table III. Solar modulation ϕ converges to zero in this case.

As can be seen that this model well explains the AMS-02 data. The best-fit radio spectral index of Vela YZ seems reasonable, as it is close to the typical value 0.5. Di Mauro *et al.* [13] also fit the four leptonic observables of AMS-02 simultaneously and obtain fairly good result. However, our model has two main differences from theirs. First, the propagation parameters they adopted is the *MED* model proposed by Ref. [101] which is based on the B/C analysis performed in Ref. [102], and the nuclei data behind is taken from earlier balloon and space experiments; as described in Sec. II A, we include the latest B/C data from AMS-02 in our calculation of propagation parameters. Besides, Vela X and YZ are assumed to provide a whole SNR contribution in their fittings. As mentioned above, these objects may not share the same spectral index, cut-off energy, and normalization parameter Q_0. If the contribution of Vela X is considered in the energy range covered by AMS-02, it should have contributed to positron intensity due to its PWN nature, and would not induce a spectral structure at high energies above TeV.

B. Vela YZ + Monogem Ring

In this model, we attempt to investigate the parameters of Vela YZ at first, rather than taking typical values as in the previous model. The geometry of Vela SNR can be sketched by two hemisphere with different scales due to the asymmetrical density distribution of its surrounding medium [103]. Vela Y and Z are located in the north-east(NE) part. Assuming the equilibrium between thermal pressure and magnetic pressure, Sushch and Hnatyk [103]

Model	γ	$Q_0[10^{50}\mathrm{GeV}^{-1}]$	c_{e+}	γ_{PWN}	η	$\phi[\mathrm{GV}]$	α_{vela}	$\chi^2/\mathrm{d.o.f}$
Vela	$2.411^{+0.005}_{-0.006}$	$1.77^{+0.04}_{-0.03}$	$0.745^{+0.033}_{-0.034}$	$1.98^{+0.08}_{-0.07}$	$0.742^{+0.044}_{-0.043}$	0	$0.519^{+0.32}_{-0.06}$	0.473

Model	γ	$Q_0[10^{50}\mathrm{GeV}^{-1}]$	c_{e+}	γ_{PWN}	η	$\phi[\mathrm{GV}]$	α_{mr}	$W_{mr}[10^{48}\mathrm{\ erg}]$	$E_{c,mr}[\mathrm{TeV}]$	$\chi^2/\mathrm{d.o.f}$
Vela + MR$_{\alpha=0.53}$	$2.602^{+0.006}_{-0.006}$	$3.52^{+0.08}_{-0.08}$	$0.956^{+0.042}_{-0.042}$	$1.89^{+0.09}_{-0.08}$	$0.646^{+0.049}_{-0.048}$	$0.351^{+0.099}_{-0.095}$	$0.551^{+0.061}_{-0.063}$	$2.89^{+0.45}_{-0.44}$	$1.04^{+14.73}_{-0.74}$	0.398
Vela + MR$_{\alpha=0.735}$	$2.569^{+0.007}_{-0.005}$	$3.17^{+0.06}_{-0.08}$	$0.930^{+0.042}_{-0.038}$	$1.90^{+0.09}_{-0.07}$	$0.656^{+0.048}_{-0.047}$	$0.304^{+0.104}_{-0.084}$	$0.484^{+0.096}_{-0.082}$	$2.13^{+0.40}_{-0.40}$	$1.13^{+11.01}_{-0.78}$	0.396

Model	γ	$Q_0[10^{50}\mathrm{GeV}^{-1}]$	c_{e+}	γ_{PWN}	η	$\phi[\mathrm{GV}]$	α_{loop}	$W_{loop}[10^{48}\mathrm{\ erg}]$	$E_{c,loop}[\mathrm{TeV}]$	$\chi^2/\mathrm{d.o.f}$
Vela + Lp1$_{\alpha=0.53}$	$2.579^{+0.007}_{-0.007}$	$2.95^{+0.07}_{-0.07}$	$0.898^{+0.040}_{-0.040}$	$1.92^{+0.09}_{-0.08}$	$0.669^{+0.048}_{-0.048}$	$0.256^{+0.106}_{-0.100}$	$0.438^{+0.028}_{-0.106}$	$4.94^{+0.58}_{-0.57}$	$1.02^{+0.97}_{-0.47}$	0.401
Vela + Lp1$_{\alpha=0.735}$	$2.580^{+0.007}_{-0.007}$	$3.00^{+0.07}_{-0.07}$	$0.907^{+0.040}_{-0.040}$	$1.91^{+0.09}_{-0.08}$	$0.665^{+0.048}_{-0.048}$	$0.265^{+0.104}_{-0.098}$	$0.417^{+0.068}_{-0.060}$	$5.08^{+0.62}_{-0.62}$	$1.49^{+1.32}_{-0.65}$	0.400

TABLE III. Fitting results of models presented in Sec. III. Loop I is abbreviated to Lp1 in this table.
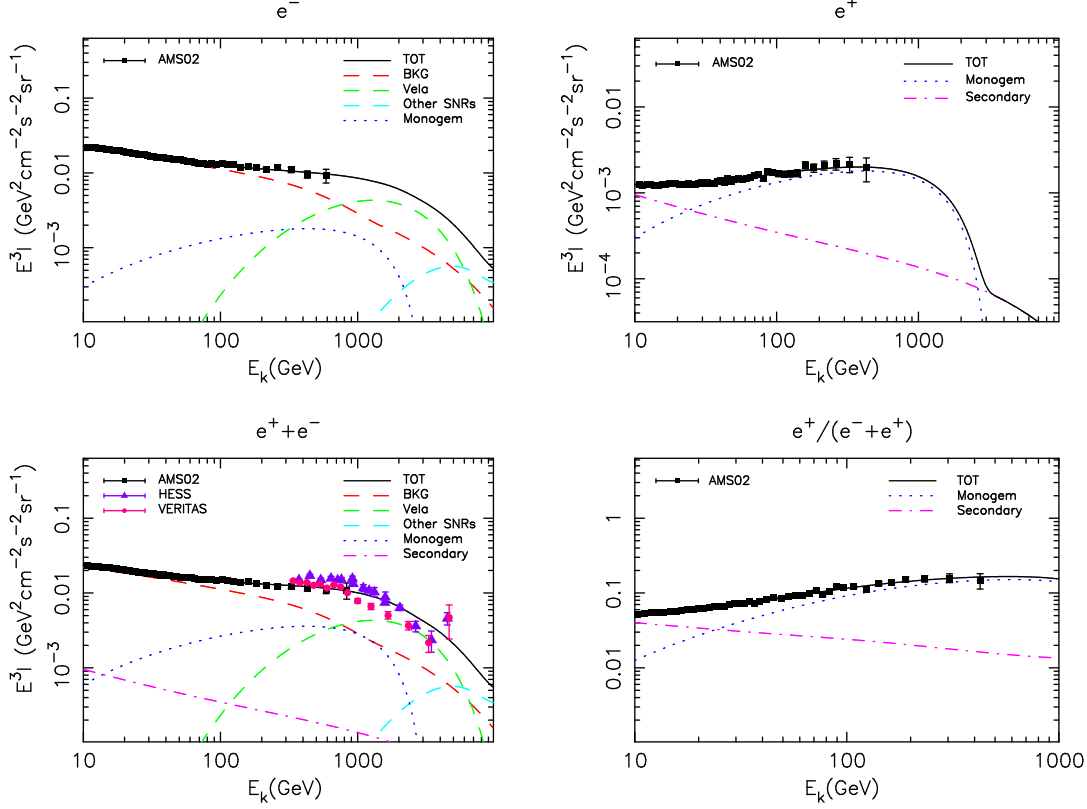
FIG. 5. The results of global fitting to AMS-02 data (*Vela YZ* model). Top left: electron intensity; top right: positron intensity; bottom left: positron plus electron intensity; bottom right: positron fraction. The legend explains different components in each sub-graph. In the legends, 'TOT' stands for total value, 'BKG' stands for SNR background, 'Other SNRs' refers to the summation of SNRs in Table II. Besides AMS-02, data from HESS and VERITAS measurements are also shown in $e^+ + e^-$ graph.

give an estimation of $B_{NE} = 46\,\mu G$ with the formula $B_{NE} = \sqrt{8\pi n_{NE} k_B T_{NE}}$, where density n_{NE} and temperature T_{NE} are derived by Ref. [104]. We still cite Eq. (14) to calculate cut-off energy. But instead of taking typical value $10^8\,\mathrm{cm\,s^{-1}}$, we choose $v_{NE} = 6 \times 10^7\,\mathrm{cm\,s^{-1}}$ estimated by Ref. [104]. The principle behind this estimation is the expression of shock radius as a function of the age of SNR given by Ref. [105]. We get $E_c = 4\,\mathrm{TeV}$. For α_r of Vela YZ, Dwarakanath [106] claims a value of 0.53 combining his 34.5 MHz observation and other observations up to 2700 MHz. The latest work about radio spectrum of Vela is done in Ref. [51]. The authors of Ref. [51] included more data points at other frequencies while subtracted the flux density at 34.5 MHz for the probable absorption of this measurement. The α_r of Vela YZ is derived to be 0.735 in this work. For $\alpha_{vela} = 0.53$, $B_r^{1\mathrm{GHz}}$ is derived to
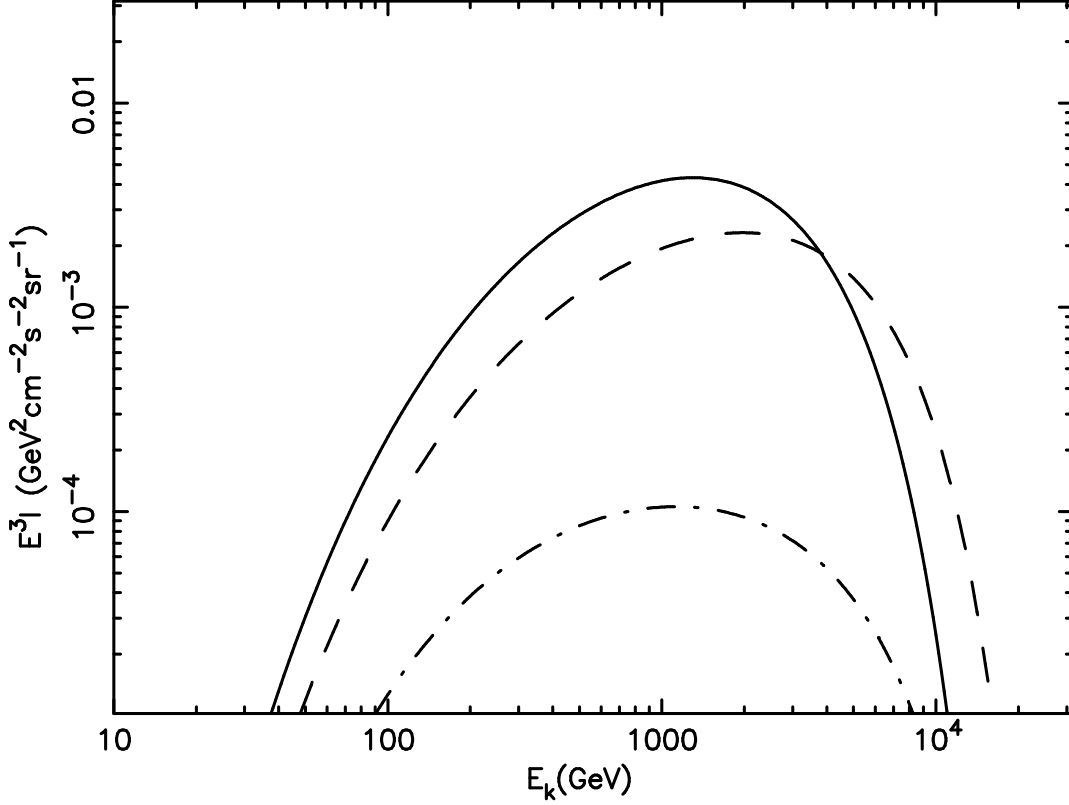
20

FIG. 6. Electron spectra of Vela YZ with different parameters. The solid line describes the case $B = 30\,\mu G$, $E_c = 2\,\mathrm{TeV}$ and $\alpha_{vela} = 0.519$. The first two are typical values and the last is given by fitting. The dashed line and the dot-dashed line come from $B = 46\,\mu G$, $E_c = 4\,\mathrm{TeV}$, $\alpha_{vela} = 0.53$ for the former and $\alpha_{vela} = 0.735$ for the later.

be 800 Jy; while for $\alpha_{vela} = 0.735$, we derive $B_r^{1\mathrm{GHz}} \sim 700\,\mathrm{Jy}$.

Fig. 6 shows the comparison between the electron spectra of Vela YZ with parameters in the previous model (solid line) and parameters in this model (dashed line for $\alpha_{vela} = 0.53$ and dot-dashed line for $\alpha_{vela} = 0.735$). If we take our parameters estimated above and still use Vela YZ as the only predominant SNR in the fitting, excesses of e^- and $e^- + e^+$ data would arise in hundreds of GeV, especially for the case $\alpha_{vela} = 0.735$. Thus, we need to find a proper SNR as a cooperator in this case. Fig. 5 indicates SNRs listed in Table II hardly have influence on electron intensity in the energy range of AMS-02, as we mentioned above. From Fig. 4, we can see Monogem ring and Loop I are the potential electron contributors up to 1 TeV. We would like to examine Monogem ring in this model.

Monogem Ring (MR) is a large shell-like structure in soft X-ray band with a diameter $\sim 25°$ [49]. Green does not include large X-ray regions with scales larger than $10°$ in his
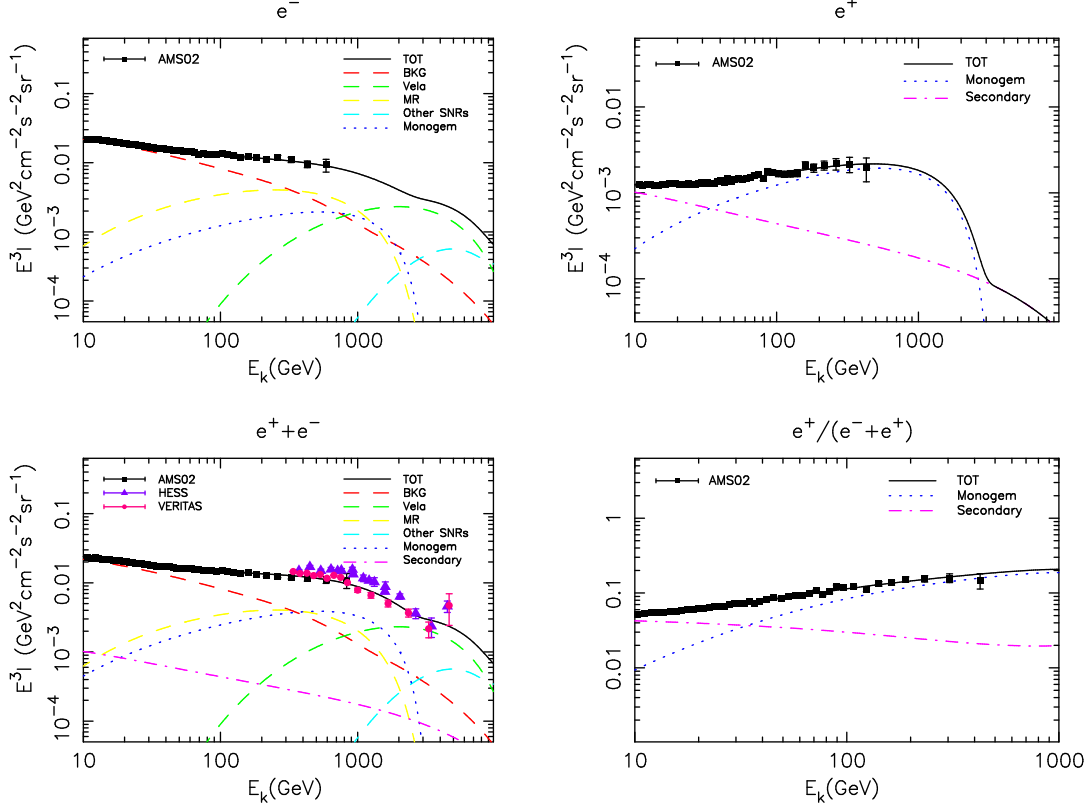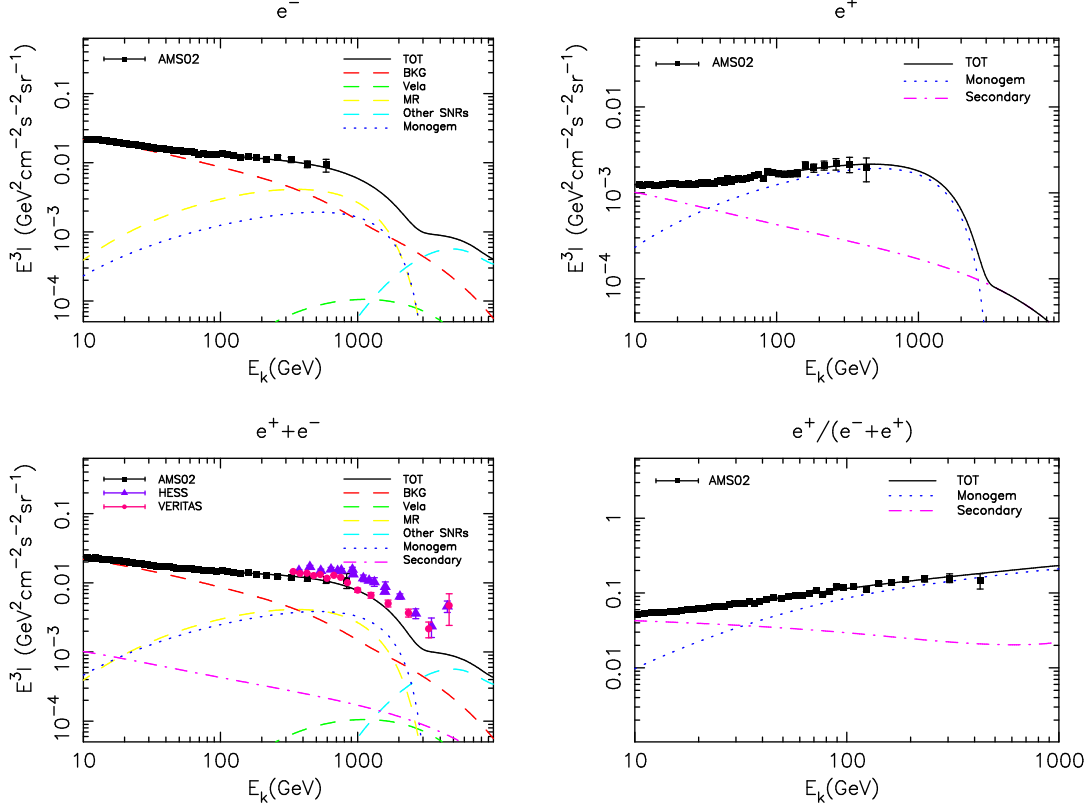
21

FIG. 7. Same as Fig. 5, but for *Vela + Monogem Ring* scenario with $\alpha_{vela} = 0.53$. In the legends, 'MR' is the abbreviation for Monogem Ring.

catalog [32], thus MR does not appear there. Assuming MR is in its adiabatic phase, Plucinsky *et al.* [49] derives parameters of MR with observable quantities and its distance, applying Sedov-Taylor model of SNR. Plucinsky [50] points out 300 pc should be a reasonable approximation for distance of MR, and consequently an age of 8.6×10^4 yr and an initial explosion energy 0.19×10^{51} erg. Apart from this, we possess poor knowledge of MR to constrain its radio spectral index, total energy converted into electrons, or cut-off energy. We add these three quantities, α_{mr}, W_{mr} and $E_{c,mr}$ to free parameters in this scenario.

Two global fittings are done with $\alpha_{vela} = 0.53$ and $\alpha_{vela} = 0.735$, and fitting results are plotted in Fig. 7 and Fig. 8 respectively. For the case $\alpha_{vela} = 0.53$, the best-fit reduced χ^2 is 0.398 for 180 d.o.f; if we take the latest value $\alpha_{vela} = 0.735$, the result becomes χ^2/d.o.f = 0.396 for 180 d.o.f. Best-fit parameters are shown in Table III for both cases. It can be seen, good fitting results to AMS-02 data are achieved when MR joins in the model. In e^- and $e^- + e^+$ spectra, the deviation between these two results with different α_{vela} becomes clear in TeV range.

22

FIG. 8. Same as Fig. 5, but for *Vela + Monogem* Ring scenario with $\alpha_{vela} = 0.735$. In the legends, 'MR' is the abbreviation for Monogem Ring.

C. Vela YZ + Loop I (NPS)

In this model, we largely repeat the work of the previous model, but replace MR by Loop I. It is well known that there are several Galactic giant radio loops potentially associating with SN events [107–109]. Loop I, which was discovered by Large *et al.* [110] and named by Berkhuijsen [111], is the most prominent one among these loops. Although Loop I, with a radius of $58°$, is also not included in the Green's catalog, it has gone through more careful study than MR. The center of Loop I is close to Scorpio-Centaurus OB association where SN events happen. North Polar Spur (NPS) is the most prominent part of Loop I, both in radio and X-ray maps [60]. However, the visible X-ray contradicts with the age of 10^6 yr derived by the low expanding velocity of H I surrounding Loop I [112, 113]. Then a reconciliation is raised: Loop I is indeed an old structure, but it has been reheated by younger SN events [60, 114]. The shock wave from the most recent SN event in Sco-Cen association happened in 2×10^5 years ago and gave rise to the X-ray feature of NPS [60]. The comparison between
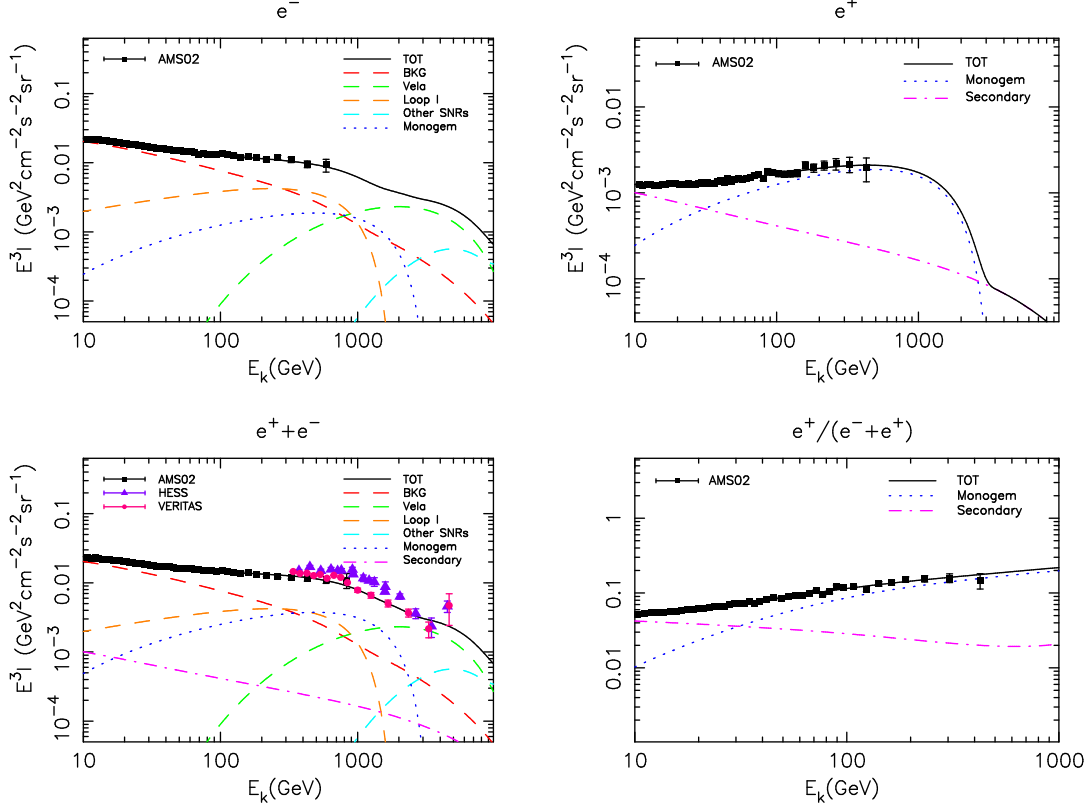
FIG. 9. Same as Fig. 5, but for *Vela + Loop I (NPS)* scenario with $\alpha_{vela} = 0.53$.

the continuous shell-like radio structure and the interrupted X-ray structure of Loop I also favors this interpretation. Thus 2×10^5 yr should be take as the age of Loop I (NPS) in our work, and adopting the corresponding distance to NPS—100 pc [59]—as the distance of this source is more reasonable than taking that of Sco-Cen association (170 pc) as in some earlier researches. Similar to the previous model, free parameters associating with Loop I (NPS) in the following fittings are α_{loop}, W_{loop} and $E_{c,loop}$.

The fitting results are shown in Fig. 9 and Fig. 10 for the case of $\alpha_{vela} = 0.53$ and $\alpha_{vela} = 0.735$, respectively. The best-fit reduced χ^2 for the former case is 0.401 for 180 d.o.f, while for the later case, $\chi^2/d.o.f = 0.400$ for 180 d.o.f. See Table III for corresponding best-fit parameters. Comparing with the reduced χ^2 of the previous model, the fitting effect of this *Vela YZ + Loop I* scenario has little difference with that of *Vela YZ + Monogem Ring* scenario.
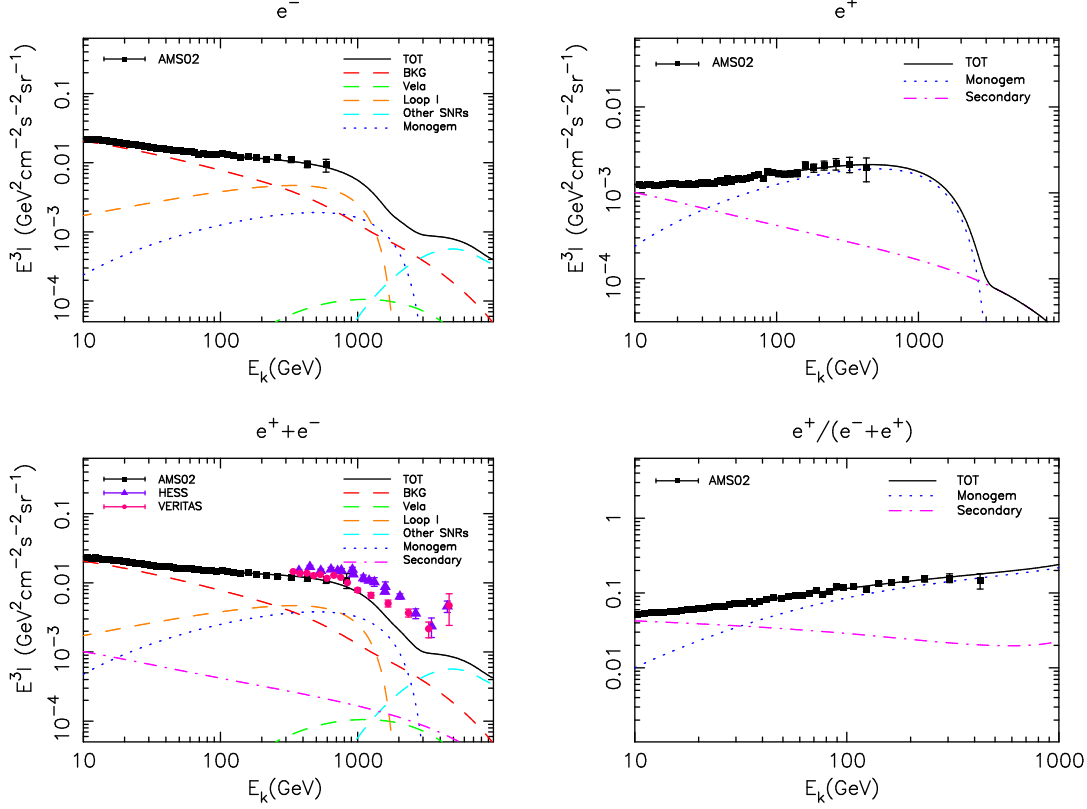
24

FIG. 10. Same as Fig. 5, but for *Vela + Loop I (NPS)* scenario with $\alpha_{vela} = 0.735$.

D. Discussion

In this section, we have proposed several source models to fit the leptonic spectra measured by AMS-02. It can be seen that the radio spectral index of Vela YZ is crucial to the situation. Radio measurements from Wilkinson Microwave Anisotropy Probe (WMAP) and Planck may give further constraints on α_{vela}, but processed data for Vela is not available at present. If the radio spectral index of Vela YZ is ~ 0.5, other local SNRs, may not be necessary to join in fitting to the AMS-02 data, as in the *Vela YZ* model. However, if we choose a value of 0.735, Vela loses its predominance of the local contribution. Since the electron intensity contributed by the PWN is confined by e^+ spectrum, other local SNRs, such as MR and Loop I, are needed to reproduce the observed e^- spectrum.

In the *Vela YZ + Monogem Ring* model, the best fitting lepton energy is 2.13×10^{48} erg, near the typical value of 10^{48} erg. However, the low explosion energy of MR derived by Plucinsky [50] favors a small input energy of electrons, or a very large conversion efficiency of $\sim 10^{-2}$ is required. For the *Vela YZ + Loop I* model, we get a larger input energy for

electrons of 5.08×10^{48} erg. However, this large value seems not excluded by the initial SN energy of Loop I of 10^{52} erg, which may be produced by several SN events [60]. Our fitting result of α_{loop} is 0.417, which is smaller than the value of 0.5 given by the radio observation to NPS between 22 and 408 MHz [115] or between 45 and 408 MHz [116]. The measurements between 408 and 1420 MHz get a even larger value of 1.1 [117]. It is also possible that both MR and Loop I play important roles in the e^- spectrum. This setting may relax the ranges of W_{mr} and α_{loop} somewhat.

IV. ELECTRON SPECTRUM ABOVE TEV

Now we turn attention to higher energy part beyond the scope of AMS-02. DAMPE is expected to detect electrons/positrons in the range of 5 GeV to 10 TeV [18]. Models proposed in the previous section have already given $e^- + e^+$ spectra extending to TeV range, which may be measured in future DAMPE data. However, although these models give different predictions in TeV range depending on the characteristic of Vela YZ, a common decreasing is shown in $e^- + e^+$ spectrum up to 10 TeV in each model. This means that these models predict no protruding structure in the highest energy range of DAMPE.

Ground-based Cherenkov telescopes, such as HESS [15, 16], MAGIC [118] and VERITAS [17], have extended the measurement of $e^- + e^+$ spectrum to several TeV. These measurements show that a spectral steepening appears above 1 TeV. Furthermore, HESS and the preliminary result of VERITAS have measured a coincident ascending of $e^- + e^+$ intensity in ~ 5 TeV, which may imply a feature from local sources. Unfortunately, this tendency comes from only the most energetic data point in both case and no measurement has been taken above 5 TeV. Thus it is the show time for DAMPE to examine this tendency.

In this section, we give additional predictions to electron spectrum above TeV. We would study whether local sources can produce distinctive features in the high energy range covered by DAMPE. Although we do not intend to fit the data of HESS, MAGIC, or VERITAS quantitively, we need to keep in mind that the spectral steepening just beyond 1 TeV could be reproduced in our models.

A. Vela X

There is still an important source which have not been included in our models so far: Vela X, as the sibling of Vela YZ. Vela X is one of the most well studied PWN powered by PSR B0833–45 [100]. It has been covered by observations from radio bands to very high energy γ-ray bands [51, 119–123]. In morphology, Vela X consists of an extended halo and a small collimated fearture embeded in the halo, e.g., the 'cocoon'. TeV γ-ray emssion has been detected in the cocoon region by HESS, while Fermi-LAT observations has reported the presence of sub-GeV-peak γ-ray emssion extending in the halo. de Jager et $al.$ [124] proposes a model with two populations of electrons to interpret this phenomenon: a high energy component concentrating on the cocoon responsible for X-ray and TeV γ-ray emssion, and a lower energy component extending in the halo responsible for radio and GeV γ-ray emssion. Following this idea, assuming the leptonic origin of γ-ray emssion, Abdo et $al.$ [122] give a multi-wavelength fitting to the SED of Vela-X. In their results, the cut-off energy of the halo is only 100 GeV which is too low to help Vela-X appearing in TeV range; for the cocoon, although its cut-off energy is high enough, a total lepton energy of 1.5×10^{46} erg is too weak to produce significant structure in TeV spectrum.

However, as mentioned above, these electron features derived by photon emission may not describe those electrons we have observed. Hinton et $al.$ [125] provide an alternative model in which a serious particle escape has happened in the halo while particles in the cocoon are well confined. After staying in confinement status for a long time, PWN begins to interact with the coming reverse shock of SNR. It is the time that PWN crushes and burst-like injection happens. From then on, the halo has been suffering from energy-dependent escape, thus the cut-off energy derived by Fermi-LAT observations is such a small value. From some moment after the PWN crushes, the pulsar starts to inject particles to a new PWN, that is, the cocoon. This explains the dimness of the cocoon for its short time of particle injection.

Hinton et $al.$ [125] gives an estimation of electron injection spectrum: $E^{1.8}\exp(E/6\,\mathrm{TeV})$ with an total energy 6.8×10^{48} erg. Thus Vela X seems to produce a TeV feature. However, the diffusion coefficient adopted by them $(1.07 \times 10^{27}(E/1\,\mathrm{GeV})^{0.6}\,\mathrm{cm}^2\,\mathrm{s}^{-1}$ for energy much larger than $1\,\mathrm{GeV})$ is almost an order of magnitude smaller than ours. If we take our $D(E)$, the intensity from Vela X is much larger, especially at lower energy. The spectral steepening
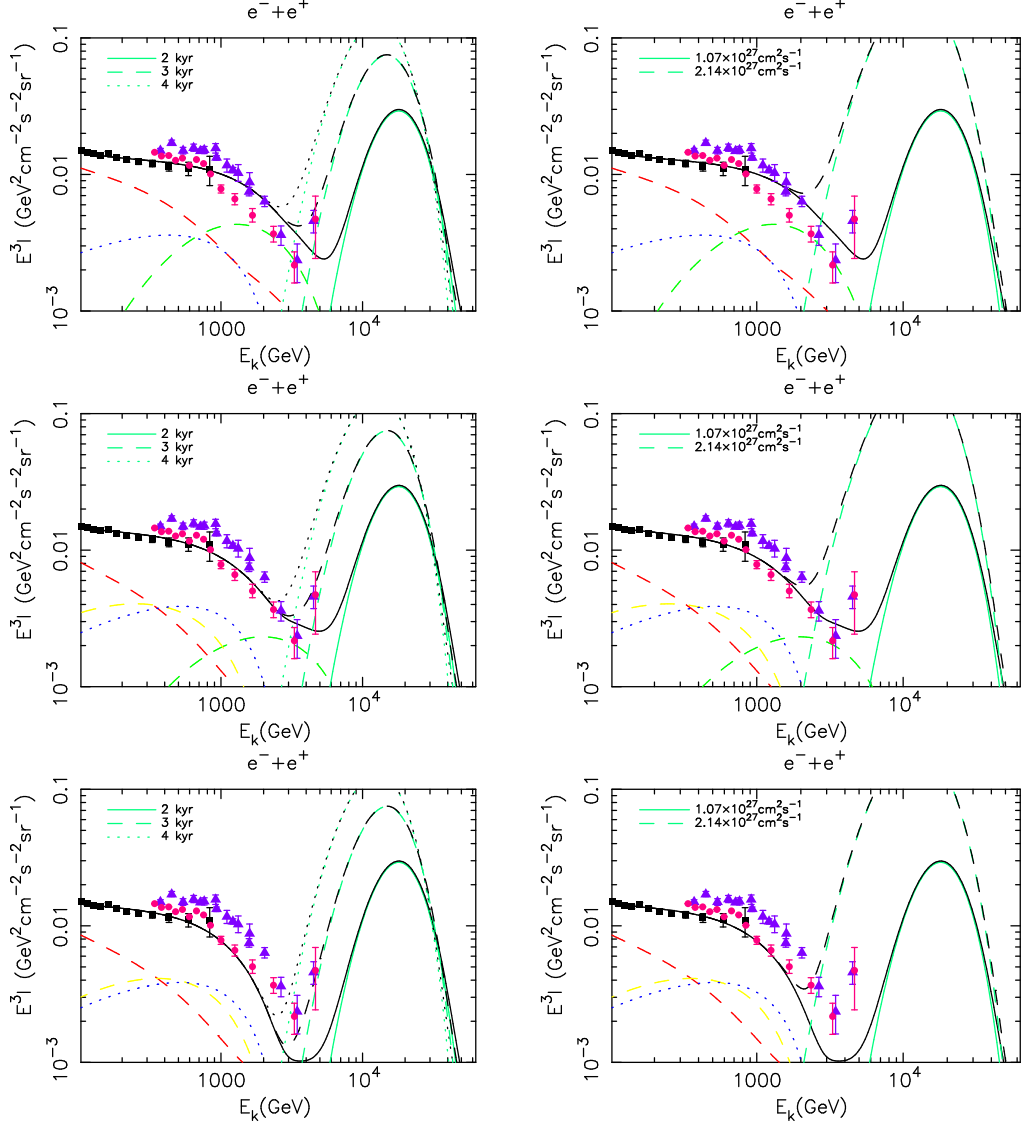
FIG. 11. Predictions to $e^- + e^+$ spectrum above TeV combining models in Sec. III and Vela X as predominant contributor in TeV range. Top left and top right: Vela X combining with *Vela YZ* model; middle left and middle right: Vela X combining with *Vela YZ + Monogem Ring* model ($\alpha_{vela} = 0.53$); bottom left and bottom right: Vela X combining with *Vela + Monogem Ring* model ($\alpha_{vela} = 0.735$). The legends in Fig. 5, 7 and 8 are still valid in this figure to describe corresponding components. Left panels show effects of varying the injection age of Vela X and right panels show effects of changing D_0.

indicated by HESS and VERITAS cannot be reproduced, and even the energy range of AMS-02 would be affected. Since the diffusion scale is proportional to $\sqrt{D(E)t}$, a larger $D(E)$ means a faster propagation and more electrons with lower energy are able to arrive

at the Earth. If we want to keep the steepening feature in 1 TeV, an unreasonable young age of Vela X is needed.

We combine Vela X and each model in the previous section to give new predictions. As discussed above, we have to keep the $D(E)$ given by Ref. [125] only for Vela X. Fig. 11 shows the predicted $e^- + e^+$ spectra. Since there is little difference between the spectral shape of *Vela YZ + MR* model and *Vela YZ + Loop I* model, we only draw the former case as representative. The effects of varying injection time of Vela X and diffusion coefficient are also shown in Fig. 11. We take three different injection age of Vela X as 2 kyr, 3 kyr, and 4 kyr. Note these ages are still observed ages, keeping consistent with those listed in Table I. With injection age increasing, the steepening structure in 1 TeV is gradually filled up. This requires an injection age less than 5 kyr, according with the theory that reverse shock has recently crushed the PWN [126]. Moreover, Fig. 11 indicates the spectrum of Vela X depends sensitively on diffusion coefficient (we double the D_0 for comparison). With the data of DAMPE and a clearer picture of the particle escape of PWN in the future, Vela X may become a potential tool to constrain diffusion coefficient in high energy.

B. Vela YZ

Naturally, following Vela X, the next question is if Vela YZ can play an important role in the highest energy part of DAMPE. The work of Ref. [12] shows the possibility of this scenario after considering the release time of electrons in SNR, although they do not make a distinction between Vela X and Vela YZ. Erlykin and Wolfendale [127] believe that electrons start their propagation after the expansion phase of SNR which hold a typical time scale of 200 yr. This time delay is too small to change the electron spectrum of Vela YZ. Alternatively, Dorfi [128] point out particles begin to escape from the shock front when the SNR dissolves in the ISM, i.e., when the velocity of the shock has dropped to the mean Alfvén velocity of ISM. However, even we take a very low number density of $0.01\,\mathrm{cm}^{-3}$, the derived release time is several times of $10^4\,\mathrm{yr}$ which is larger than the observed age of Vela YZ or the typical time scale of Sedov phase. To insure electrons have already escaped from Vela YZ, we should control its release time not longer than $10^4\,\mathrm{yr}$, corresponding to a least observed age 1 kyr. The total input energy of Vela YZ is much smaller than that of Vela X, it should be at the magnitude of 10^{47} erg. When the electron acceleration is synchrotron loss limited,
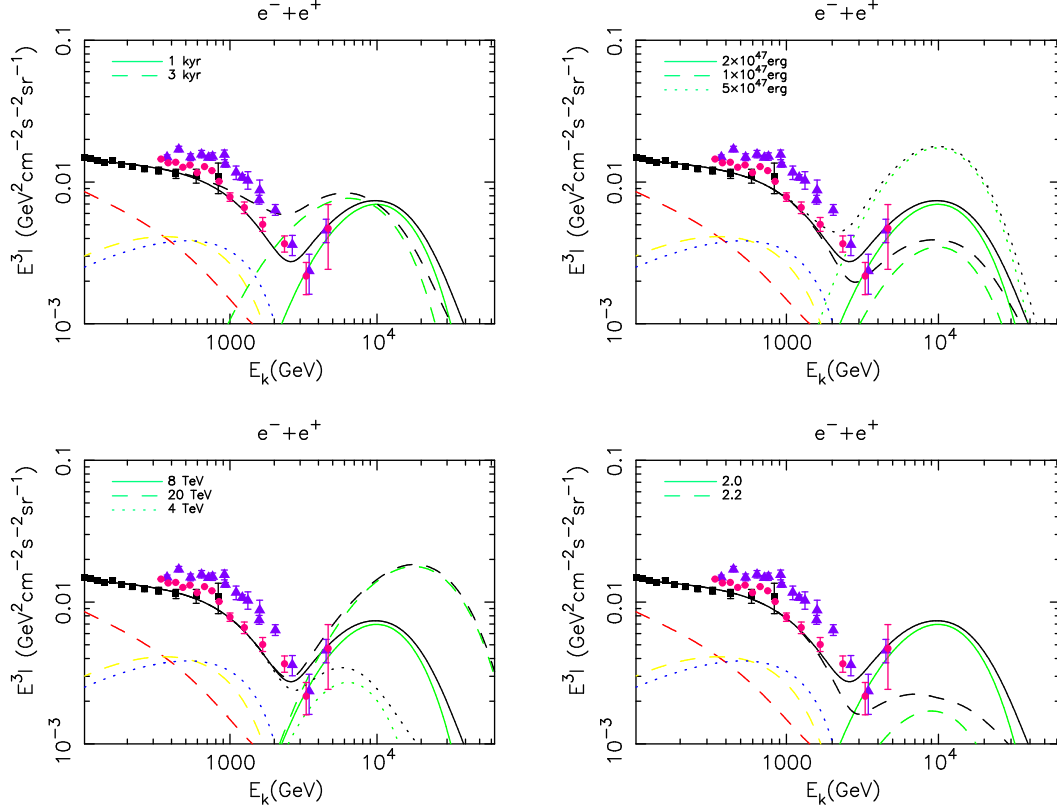
FIG. 12. Predictions to $e^- + e^+$ spectrum above TeV replacing the Vela YZ in *Vela YZ + Monogem Ring* model ($\alpha_{vela} = 0.735$) with the Vela YZ estimated in Sec. IV B. Top left: effect of varying observed age of Vela YZ; top right: effect of varying input energy of leptons of Vela YZ; bottom left: effect of varying cut-off energy of Vela YZ; bottom right: effect of varying electron spectral index of injection spectrum of Vela YZ. Black lines in each graph stand for total intensity corresponding to the Vela YZ with same line style, and solid green line in each graph represents Vela YZ adopting our fiducial parameters: $t = 1\,\text{kyr}$, $W = 2 \times 10^{47}\,\text{erg}$, $E_c = 8\,\text{TeV}$ and $\gamma = 2.0$. The legends in Fig. 8 are still valid in this figure to describe corresponding components.

the cut-off energy decreases with the age growth of SNR. Since $E_c = 4\,\text{TeV}$ is derived by observations of electromagnetic radiation, the injection spectrum of electrons should have a larger cut-off energy. Similarly, higher energy electrons should suffer heavier energy loss, which causes softening of spectrum with the growth of trapped time of electrons. Thus the spectral index of injection spectrum may smaller than that derived by radio observations.

We set $t = 1\,\text{kyr}$, $W = 2 \times 10^{47}\,\text{erg}$, $E_c = 8\,\text{TeV}$ and $\gamma = 2.0$ as fiducial values and use some other values of these parameters to show spectral variation in Fig. 12. In this figure, we apply *Vela YZ + Monogem Ring* model ($\alpha_{vela} = 0.735$) in Sec. III. In this model Vela

30

YZ can bring ascending or relatively flat spectral features just below 10 TeV, as shown in Fig. 12. We can imply from this figure that if the radio spectral index is taken 0.735 here, Vela YZ will have no chance to produce spectral feature in $\sim$ TeV.

C. Vela Jr.

Besides Vela XYZ, other candidates producing prominent structure in the TeV range should be selected from Table II. Fig. 13 shows intensity of each SNR listed in Table II, along with the data of HESS and VERITAS. Cygnus Loop and HB9 do not appear in the scope of Fig. 13 because of their very low cut-off energy. To affect the $e^- + e^+$ spectrum in $\sim$ TeV, Vela Jr. seems to need least parametric adjustment, namely, a larger input energy to leptons. Thus we examine Vela Jr. as an example.

Vela Jr. locates in the southeastern corner of Vela on the sky map, but at a farther distance of 750 pc. Vela Jr. is one of those sources whose parameters are estimated by fitting the multi-wavelength emission in Sec. II B 2. Tanaka *et al.* [79] and Lee *et al.* [129] also conducted broadband analysis to Vela Jr. in recent years. As there have been discussions about magnetic field of Vela Jr., Q_0 and E_c can be estimated by Eq. (12) and Eq. (14). We put aside our fitting result to parameters of Vela Jr. temporarily. Chandra has detected spindly filamentary structure in Vela Jr. [130]. This thin structure is interpreted by efficient synchrotron cooling of CR electrons in a strong local magnetic field of $\sim$ 100 μG [131]. However, if broadband emission is modeled by leptonic scenario, a magnetic field of $\sim$ 10 μG is required to explain the synchrotron to inverse Compton flux ratio. Thus we take three different magnetic fields of 100 μG, 10 μG and a typical value 30 μG adopted in Ref. [13]. Here α_r and $B_r^{1\mathrm{GHz}}$ are taken to be 0.3 and 50 Jy, as given in Table I, to calculate Q_0. We take the upper limit of the age of Vela Jr., i.e. an observed age of 4.3 kyr.

The predicted $e^- + e^+$ spectrum of Vela Jr. combining with *Vela YZ* and *Vela YZ + Monogem Ring* models (of course original Vela Jr. subtracted) are shown in Fig. 14. The input leptonic energy corresponding to magnetic field of 30 μG, 100 μG and 10 μG are 1.72×10^{48} erg, 2.80×10^{47} erg and 8.92×10^{48} erg, respectively. For the case of $B = 100\,\mu$G, Vela Jr. cannot produce prominent feature in $\sim$ TeV; when $B = 10\,\mu$G, the spectral feature given by Vela Jr. is remarkable enough, but it needs a total leptonic energy much higher than the typical value of 10^{48} erg. The result given by $B = 30\,\mu$G may be what we'd like
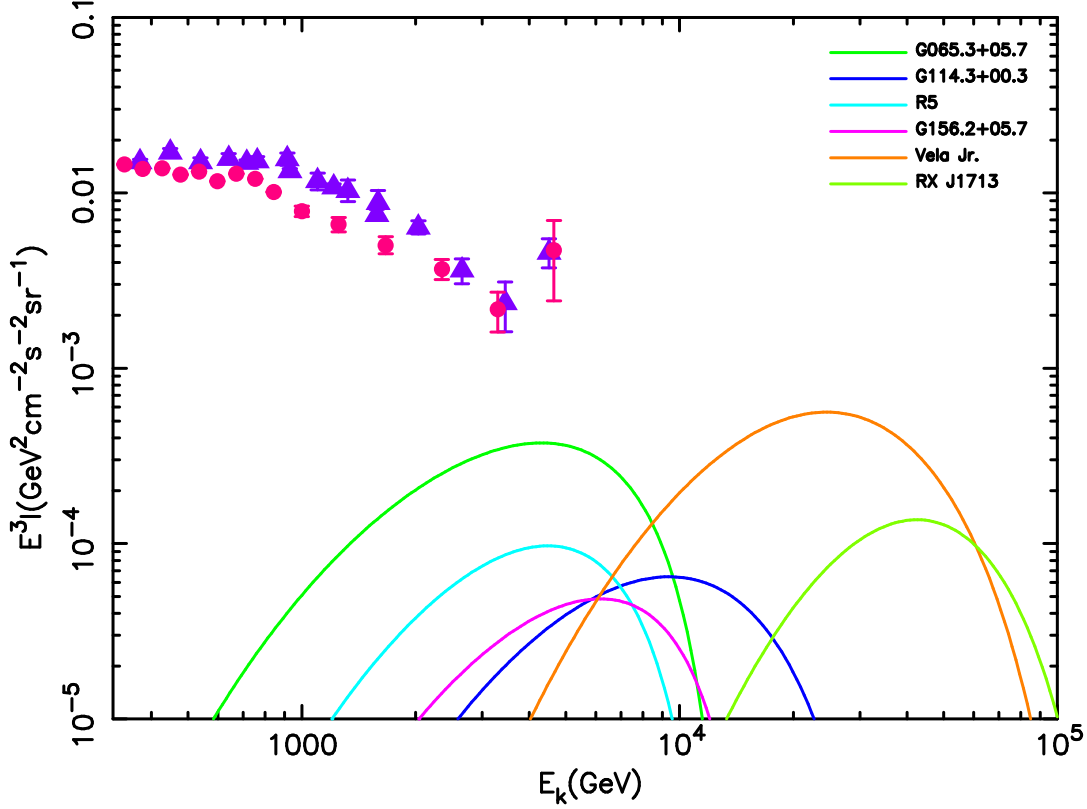
FIG. 13. Electron intensities of individual local SNRs listed in Table II. Cygnus loop and HB9 do not appear in the scope of this figure because of their very low cut-off energy, as shown in Table II. Data from HESS and VERITAS measurements are also shown in this figure.

to see. However, we should note the α_r of Vela Jr. is derived by the radio flux of only two wave bands, which is quite unreliable, and the value of α_r will give a significant influence to the total leptonic energy of Vela Jr. with the method used here. In fact, the parameters given by the leptonic model of Ref. [79] is similar to the result of our broadband fitting (the differences may be due to the consideration of the energy loss between injection electrons and radiation electrons in the work of [79]). Lee *et al.* [129] also found the leptonic model is clearly superior to hadronic model. Thus broadband fitting may give better constraint to parameters of Vela Jr., which disfavor Vela Jr. as a prominent contributor in $\sim$ TeV.

D. Cygnus Loop

Cygnus Loop is one of the closest SNRs to the Earth (540 pc) and is considered as an important local CR accelerator second only to Vela [13]. However, its steep GeV spectrum
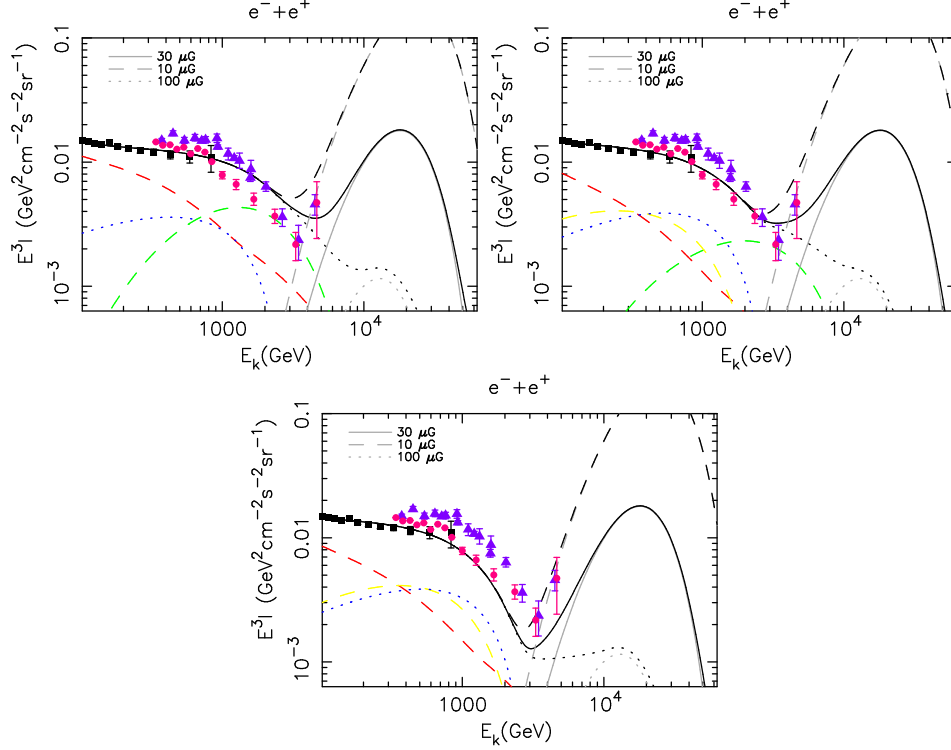
FIG. 14. Predictions to $e^- + e^+$ spectrum above TeV combining models in Sec. III and Vela Jr. as predominant contributor in TeV range. Top left: Vela Jr. combining with *Vela YZ* model; top right: Vela Jr. combining with *Vela YZ + Monogem Ring* model ($\alpha_{vela} = 0.53$); bottom: Vela Jr. combining with *Vela + Monogem Ring* model ($\alpha_{vela} = 0.735$). The legends in Fig. 5, 7 and 8 are still valid in this figure to describe corresponding components. Effects of adopting different magnetic field are shown in these graphs. Black lines in each graph stand for the total intensity corresponding to the Vela Jr. with the same line style.

observed by Fermi-LAT (see Fig. 3) indicates a very low cut-off energy of electron spectrum, thus it cannot play a part in the models above. Cut-off energy derived by Eq. (14) is at least several TeV for Cygnus Loop, so it is possible that Cygnus Loop has undergone serious particle escape similar to the case of Vela X. Unfortunately, although Cygnus Loop has been carefully studied in X-ray band with the help of XMM-Newton and Suzaku [132, 133], its global X-ray spectrum is not available. Thus we cannot give further inference from the broadband spectrum of Cygnus Loop as Vela X. Here we assume cut-off energy of TeV for Cygnus Loop, which is the precondition for Cygnus Loop to contribute significantly in TeV range. Besides, to preserve the spectral steepening in 1 TeV, considerable release time is needed for Cygnus Loop. We keep others parameters given by broadband fitting unchanged.
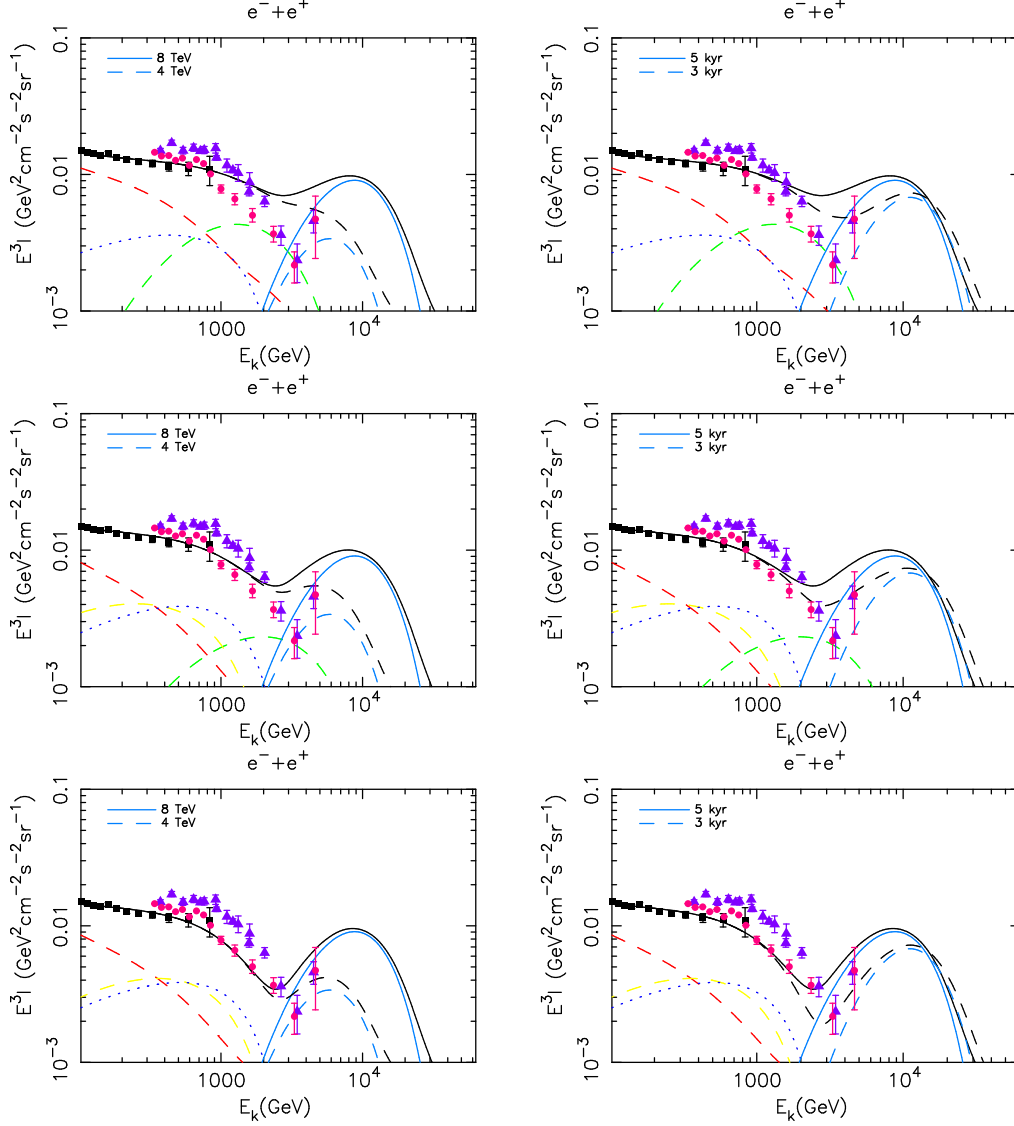
FIG. 15. Same as Fig. 11, but replace Vela X with Cygnus Loop. Left panels show effects of varying the cut-off energy of Cygnus Loop and right panels show effects of changing the injection time.

Like the former cases, we combine Cygnus Loop with models given in Sec. III and also show the effects of varying cut-off energy and observed age of Cygnus Loop in Fig. 15. In the left panels, observed age is fixed at 5 kyr, while in the right panels, cut-off energy of Cygnus Loop is set to be 8 TeV.

E. Discussion

As discussed in the last section, it is hard to tell which local SNR dominates the electron excess in the energy range of AMS-02, since the spectra of local SNRs are mixed with that of the SNR background below 1 TeV. However, things are different above the TeV scale that can be covered by DAMPE. The contributions from the background SNRs may be very small in this energy range. If we get a distinctive spectrum above several TeV, we may determine the origin of these cosmic ray electrons. Of course, it is also possible that more than one sources shape the high energy electron spectrum, then the situation becomes complicated.

In order to produce clear features at the spectrum beyond TeV, a small particle propagation time and a high energy cut-off of injection electrons are essential. We have considered the Vela X, Vela YZ, Vela Jr. and Cygnus Loop as possible candidates contributing to cosmic electrons above TeV in this section. Except for very young sources like Vela Jr., other three candidates need an additional release time. We find that Vela X and Vela Jr. may provide a very sharp rise in the spectrum at a few TeV due to the very young components, while the Vela YZ and Cygnus Loop may show much smoother feature at the similar energy. Thus with the basis of a $\sim$ kyr injection age and a $\sim$ TeV cut-off energy, the total leptonic injection energy of a source is the key factor to produce a sharp spectral structure in the high energy range covered by DAMPE.

V. SUMMARY

In this paper, we have given predictions to CR electron (plus positron) spectrum above $\sim$ TeV basing on the elaborate analysis of the local astrophysical sources, especially the local SNRs. In order to obtain a complete picture, we ensure the consistency between the predicted spectra and present experimental results below TeV by performing global fittings to all the latest leptonic AMS-02 data. We find that Vela YZ could act as the dominator just below TeV because of its proper age and distance. However, it should be emphasized that the determination of the injection spectral index of Vela YZ, which still has some uncertainties, is crucial to fittings. We discuss different scenarios to fit AMS-02 data corresponding to different values of the spectral index of Vela YZ. Other SNRs, such as Monogem Ring and Loop I, are also introduced, if Vela YZ dose not provide the dominant contribution to the

AMS-02 electron results.

Basing on the fitting results, we discuss the parameters of several local sources, and give further expectations of the electron spectrum above TeV. Adopting different possible values for those parameters, we predict either sharp or relatively flat electron spectral features, comparing with the monotonic decreasing spectra of the models in Sec. III. All these models are ready for the examination at high energy CR electron detectors, such as DAMPE, which can reach the energy as high as ~ 10 TeV. The spectrum measurement of DAMPE and future anisotropy measurements [134] may reveal the origin of the high energy CR electrons. These results will also be important for probing the mechanism of CR acceleration in the sources.

ACKNOWLEDGMENTS

[1] M. Aguilar, G. Alberti, B. Alpat, A. Alvino, G. Ambrosi, K. Andeen, H. Anderhub, L. Arruda, P. Azzarello, A. Bachlechner, *et al.*, Physical Review Letters **110**, 141102 (2013).

[2] O. Adriani *et al.*, Nature **458**, 607 (2009), arXiv:0810.4995.

[3] O. Adriani *et al.*, Physical Review Letters **106**, 201101 (2011), arXiv:1103.2880 [astro-ph.HE].

[4] A. A. Abdo *et al.*, Physical Review Letters **102**, 181101 (2009), arXiv:0905.0025 [astro-ph.HE].

[5] M. Ackermann *et al.*, Phys. Rev. D **82**, 092004 (2010), arXiv:1008.3999 [astro-ph.HE].

[6] J. Chang, J. H. Adams, H. S. Ahn, G. L. Bashindzhagyan, M. Christl, O. Ganel, T. G. Guzik, J. Isbert, K. C. Kim, E. N. Kuznetsov, M. I. Panasyuk, A. D. Panov, W. K. H. Schmidt, E. S. Seo, N. V. Sokolskaya, J. W. Watts, J. P. Wefel, J. Wu, and V. I. Zatsepin, Nature **456**, 362 (2008).

[7] L. Feng, R.-Z. Yang, H.-N. He, T.-K. Dong, Y.-Z. Fan, and J. Chang, Physics Letters B **728**, 250 (2014), arXiv:1303.0530 [astro-ph.HE].

[8] X. Li, Z.-Q. Shen, B.-Q. Lu, T.-K. Dong, Y.-Z. Fan, L. Feng, S.-M. Liu, and J. Chang, Physics Letters B **749**, 267 (2015), arXiv:1412.1550 [astro-ph.HE].

[9] S.-J. Lin, Q. Yuan, and X.-J. Bi, Phys. Rev. D **91**, 063508 (2015), arXiv:1409.6248 [astro-ph.HE].

[10] C. S. Shen, Astrophys. J. Lett. **162**, L181 (1970).

[11] A. M. Atoyan, F. A. Aharonian, and H. J. Völk, Phys. Rev. D **52**, 3265 (1995).

[12] T. Kobayashi, Y. Komori, K. Yoshida, and J. Nishimura, Astrophys. J. **601**, 340 (2004), astro-ph/0308470.

[13] M. Di Mauro, F. Donato, N. Fornengo, R. Lineros, and A. Vittino, J. Cosmol. Astropart. Phys. **4**, 006 (2014), arXiv:1402.0321 [astro-ph.HE].

[14] G. Jóhannesson, R. Ruiz de Austri, A. C. Vincent, I. V. Moskalenko, E. Orlando, T. A. Porter, A. W. Strong, R. Trotta, F. Feroz, P. Graff, and M. P. Hobson, Astrophys. J. **824**, 16 (2016), arXiv:1602.02243 [astro-ph.HE].

[15] F. Aharonian *et al.*, Physical Review Letters **101**, 261104 (2008), arXiv:0811.3894.

[16] F. Aharonian *et al.*, Astron. Astrophys. **508**, 561 (2009), arXiv:0905.0105 [astro-ph.HE].

[17] D. Staszak and for the VERITAS Collaboration, ArXiv e-prints (2015), arXiv:1508.06597 [astro-ph.HE].

[18] J. Chang, Chin. J. Space Sci. **34**, 550 (2014).

[19] T. Delahaye, J. Lavalle, R. Lineros, F. Donato, and N. Fornengo, Astron. Astrophys. **524**, A51 (2010), arXiv:1002.1910 [astro-ph.HE].

[20] A. J. Davis, R. A. Mewaldt, W. R. Binns, E. R. Christian, A. C. Cummings, J. S. George, P. L. Hink, R. A. Leske, T. T. von Rosenvinge, M. E. Wiedenbeck, and N. E. Yanasak, in *Acceleration and Transport of Energetic Particles Observed in the Heliosphere*, American Institute of Physics Conference Series, Vol. 528, edited by R. A. Mewaldt, J. R. Jokipii, M. A. Lee, E. Möbius, and T. H. Zurbuchen (2000) pp. 421–424.

[21] AMS-02 collaboration, in *International Cosmic Ray Conference* (2013).

[22] J. J. Connell, Astrophys. J. Lett. **501**, L59 (1998).

[23] N. E. Yanasak, M. E. Wiedenbeck, R. A. Mewaldt, A. J. Davis, A. C. Cummings, J. S. George, R. A. Leske, E. C. Stone, E. R. Christian, T. T. von Rosenvinge, W. R. Binns, P. L.

Hink, and M. H. Israel, Astrophys. J. **563**, 768 (2001).

[24] A. Lukasiak, International Cosmic Ray Conference **3**, 41 (1999).

[25] J. A. Simpson and M. Garcia-Munoz, Space Sci. Rev. **46**, 205 (1988).

[26] T. Hams, L. M. Barbier, M. Bremerich, E. R. Christian, G. A. de Nolfo, S. Geier, H. Göbel, S. K. Gupta, M. Hof, W. Menn, R. A. Mewaldt, J. W. Mitchell, S. M. Schindler, M. Simon, and R. E. Streitmatter, Astrophys. J. **611**, 892 (2004).

[27] R. Schlickeiser and J. Ruppel, New Journal of Physics **12**, 033044 (2010), arXiv:0908.2183 [astro-ph.HE].

[28] V. L. Ginzburg and V. S. Ptuskin, Reviews of Modern Physics **48**, 161 (1976).

[29] D. Malyshev, I. Cholis, and J. Gelfand, Phys. Rev. D **80**, 063005 (2009), arXiv:0903.1310 [astro-ph.HE].

[30] D. R. Lorimer, in *Young Neutron Stars and Their Environments*, IAU Symposium, Vol. 218, edited by F. Camilo and B. M. Gaensler (2004) p. 105, astro-ph/0308501.

[31] A. W. Strong and I. V. Moskalenko, Astrophys. J. **509**, 212 (1998), astro-ph/9807150.

[32] D. A. Green, Bulletin of the Astronomical Society of India **42**, 47 (2014), arXiv:1409.0637 [astro-ph.HE].

[33] P. W. Gorham, P. S. Ray, S. B. Anderson, S. R. Kulkarni, and T. A. Prince, Astrophys. J. **458**, 257 (1996).

[34] F. Mavromatakis, P. Boumis, J. Papamastorakis, and J. Ventura, Astron. Astrophys. **388**, 355 (2002), astro-ph/0204079.

[35] L. Xiao, W. Reich, E. Fürst, and J. L. Han, Astron. Astrophys. **503**, 827 (2009), arXiv:0904.3170.

[36] W. P. Blair, R. Sankrit, and J. C. Raymond, Astron. J. **129**, 2268 (2005).

[37] X. H. Sun, W. Reich, J. L. Han, P. Reich, and R. Wielebinski, Astron. Astrophys. **447**, 937 (2006), astro-ph/0510509.

[38] J. L. Han, W. Reich, X. H. Sun, X. Y. Gao, L. Xiao, W. B. Shi, P. Reich, and R. Wielebinski, International Journal of Modern Physics Conference Series **23**, 82 (2013), arXiv:1202.1875.

[39] R. Kothes, K. Fedotov, T. J. Foster, and B. Uyanıker, Astron. Astrophys. **457**, 1081 (2006).

[40] A. Yar-Uyaniker, B. Uyaniker, and R. Kothes, Astrophys. J. **616**, 247 (2004), astro-ph/0408386.

[41] G. Joncas, R. S. Roger, and P. E. Dewdney, Astron. Astrophys. **219**, 303 (1989).

[42] D. Leahy and W. Tian, Astron. Astrophys. **451**, 251 (2006), astro-ph/0601487.

[43] S. Katsuda, R. Petre, U. Hwang, H. Yamaguchi, K. Mori, and H. Tsunemi, Publications of the Astronomical Society of Japan **61**, S155 (2009), arXiv:0902.1782.

[44] W. Reich, E. Fuerst, and E. M. Arnal, Astron. Astrophys. **256**, 214 (1992).

[45] J. W. Xu, J. L. Han, X. H. Sun, W. Reich, L. Xiao, P. Reich, and R. Wielebinski, Astron. Astrophys. **470**, 969 (2007).

[46] S. Yamauchi, J. Yokogawa, H. Tomida, K. Koyama, and K. Tamura, in *Broad Band X-ray Spectra of Cosmic Sources*, edited by K. Makishima, L. Piro, and T. Takahashi (2000) p. 567.

[47] D. A. Leahy and W. W. Tian, Astron. Astrophys. **461**, 1013 (2007), astro-ph/0606598.

[48] W. Reich, X. Zhang, and E. Fürst, Astron. Astrophys. **408**, 961 (2003).

[49] P. P. Plucinsky, S. L. Snowden, B. Aschenbach, R. Egger, R. J. Edgar, and D. McCammon, Astrophys. J. **463**, 224 (1996).

[50] P. P. Plucinsky, in *American Institute of Physics Conference Series*, Vol. 1156, edited by R. K. Smith, S. L. Snowden, and K. D. Kuntz (2009) pp. 231–235.

[51] H. Alvarez, J. Aparici, J. May, and P. Reich, Astron. Astrophys. **372**, 636 (2001).

[52] P. A. Caraveo, A. De Luca, R. P. Mignani, and G. F. Bignami, Astrophys. J. **561**, 930 (2001), astro-ph/0107282.

[53] A. N. Cha, K. R. Sembach, and A. C. Danks, Astrophys. J. Lett. **515**, L25 (1999), astro-ph/9902230.

[54] M. Miceli, F. Bocchino, and F. Reale, Astrophys. J. **676**, 1064-1072 (2008), arXiv:0712.3017.

[55] B. Aschenbach, Nature **396**, 141 (1998).

[56] A. F. Iyudin, V. Schönfelder, K. Bennett, H. Bloemen, R. Diehl, W. Hermsen, G. G. Lichti, R. D. van der Meulen, J. Ryan, and C. Winkler, Nature **396**, 142 (1998).

[57] S. Katsuda, H. Tsunemi, and K. Mori, Astrophys. J. Lett. **678**, L35 (2008), arXiv:0803.3266.

[58] M. P. Redman and J. Meaburn, Mon. Not. Roy. Astron. Soc. **356**, 969 (2005).

[59] R. G. Bingham, Mon. Not. Roy. Astron. Soc. **137**, 157 (1967).

[60] R. J. Egger and B. Aschenbach, Astron. Astrophys. **294**, L25 (1995), astro-ph/9412086.

[61] J. S. Lazendic, P. O. Slane, B. M. Gaensler, S. P. Reynolds, P. P. Plucinsky, and J. P.

Hughes, Astrophys. J. **602**, 271 (2004), astro-ph/0310696.

[62] G. Morlino, E. Amato, and P. Blasi, Mon. Not. Roy. Astron. Soc. **392**, 240 (2009), arXiv:0810.0094.

[63] Q. Yuan, S. Liu, Z. Fan, X. Bi, and C. L. Fryer, Astrophys. J. **735**, 120 (2011), arXiv:1011.0145 [astro-ph.HE].

[64] T. A. Porter, I. V. Moskalenko, and A. W. Strong, Astrophys. J. Lett. **648**, L29 (2006), astro-ph/0607344.

[65] V. Petrosian and S. Liu, Astrophys. J. **610**, 550 (2004), astro-ph/0401585.

[66] V. Zabalza, ArXiv e-prints (2015), arXiv:1509.03319 [astro-ph.HE].

[67] D. Foreman-Mackey, D. W. Hogg, D. Lang, and J. Goodman, Publications of the Astronomical Society of Pacific **125**, 306 (2013), arXiv:1202.3665 [astro-ph.IM].

[68] R. Beck and M. Krause, Astronomische Nachrichten **326**, 414 (2005), astro-ph/0507367.

[69] B. Arbutina, D. Urošević, M. Andjelić, and M. Pavlović, Mem. S.A.It. **82**, 822 (2011).

[70] A. G. Pacholczyk, *Series of Books in Astronomy and Astrophysics, San Francisco: Freeman, 1970* (1970).

[71] R. Yamazaki, K. Kohri, A. Bamba, T. Yoshida, T. Tsuribe, and F. Takahara, Mon. Not. Roy. Astron. Soc. **371**, 1975 (2006), astro-ph/0601704.

[72] H. Katagiri, L. Tibaldo, J. Ballet, F. Giordano, I. A. Grenier, T. A. Porter, M. Roth, O. Tibolla, Y. Uchiyama, and R. Yamazaki, Astrophys. J. **741**, 44 (2011), arXiv:1108.1833 [astro-ph.HE].

[73] I. Reichardt, R. Terrier, J. West, S. Safi-Harb, E. de Oña-Wilhelmi, and J. Rico, ArXiv e-prints (2015), arXiv:1502.03053 [astro-ph.HE].

[74] B. Uyanıker, W. Reich, A. Yar, and E. Fürst, Astron. Astrophys. **426**, 909 (2004), astro-ph/0409176.

[75] M. Araya, Mon. Not. Roy. Astron. Soc. **444**, 860 (2014), arXiv:1405.4554 [astro-ph.HE].

[76] K. S. Dwarakanath, R. K. Shevgaonkar, and C. V. Sastry, Journal of Astrophysics and Astronomy **3**, 207 (1982).

[77] F. Aharonian *et al.*, Astrophys. J. **661**, 236 (2007), astro-ph/0612495.

[78] A. R. Duncan and D. A. Green, Astron. Astrophys. **364**, 732 (2000), astro-ph/0009289.

[79] T. Tanaka, A. Allafort, J. Ballet, S. Funk, F. Giordano, J. Hewitt, M. Lemoine-

Goumard, H. Tajima, O. Tibolla, and Y. Uchiyama, Astrophys. J. Lett. **740**, L51 (2011), arXiv:1109.4658 [astro-ph.HE].

[80] A. A. Abdo *et al.*, Astrophys. J. **734**, 28 (2011), arXiv:1103.5727 [astro-ph.HE].

[81] H.E.S.S. Collaboration, A. Abramowski, *et al.*, Astron. Astrophys. **531**, A81 (2011), arXiv:1105.3206 [astro-ph.HE].

[82] F. Acero, J. Ballet, A. Decourchelle, M. Lemoine-Goumard, M. Ortega, E. Giacani, G. Dubner, and G. Cassam-Chenaï, Astron. Astrophys. **505**, 157 (2009), arXiv:0906.1073 [astro-ph.HE].

[83] S. Federici, M. Pohl, I. Telezhinsky, A. Wilhelm, and V. V. Dwarkadas, Astron. Astrophys. **577**, A12 (2015), arXiv:1502.06355 [astro-ph.HE].

[84] T. Tanaka, Y. Uchiyama, F. A. Aharonian, T. Takahashi, A. Bamba, J. S. Hiraga, J. Kataoka, T. Kishishita, M. Kokubun, K. Mori, K. Nakazawa, R. Petre, H. Tajima, and S. Watanabe, Astrophys. J. **685**, 988-1004 (2008), arXiv:0806.1490.

[85] S. Della Torre, M. Gervasi, P. G. Rancoita, D. Rozza, and A. Treves, ArXiv e-prints (2013), arXiv:1307.5197 [astro-ph.HE].

[86] M. J. Rees and J. E. Gunn, Mon. Not. Roy. Astron. Soc. **167**, 1 (1974).

[87] B. M. Gaensler and P. O. Slane, Annu. Rev. Astron. Astrophys. **44**, 17 (2006), astro-ph/0601081.

[88] J. H. Taylor, R. N. Manchester, and A. G. Lyne, Astrophys. J. Supp. **88**, 529 (1993).

[89] F. Pacini and M. Salvati, Astrophys. J. **186**, 249 (1973).

[90] T. Delahaye, R. Lineros, F. Donato, N. Fornengo, J. Lavalle, P. Salati, and R. Taillet, Astron. Astrophys. **501**, 821 (2009), arXiv:0809.5268.

[91] Y. Shikaze, S. Haino, K. Abe, H. Fuke, T. Hams, K. C. Kim, Y. Makida, S. Matsuda, J. W. Mitchell, A. A. Moiseev, J. Nishimura, M. Nozaki, S. Orito, J. F. Ormes, T. Sanuki, M. Sasaki, E. S. Seo, R. E. Streitmatter, J. Suzuki, K. Tanaka, T. Yamagami, A. Yamamoto, T. Yoshida, and K. Yoshimura, Astroparticle Physics **28**, 154 (2007), astro-ph/0611388.

[92] T. Kamae, N. Karlsson, T. Mizuno, T. Abe, and T. Koi, Astrophys. J. **647**, 692 (2006), astro-ph/0605581.

[93] J. W. Norbury and L. W. Townsend, Nuclear Instruments and Methods in Physics Research B **254**, 187 (200 nucl-th/0612081.

[94] L. Accardo, M. Aguilar, D. Aisa, A. Alvino, G. Ambrosi, K. Andeen, L. Arruda, N. Attig,

P. Azzarello, A. Bachlechner, *et al.*, Physical Review Letters **113**, 121101 (2014).

[95] M. Aguilar, D. Aisa, A. Alvino, G. Ambrosi, K. Andeen, L. Arruda, N. Attig, P. Azzarello, A. Bachlechner, F. Barao, *et al.*, Physical Review Letters **113**, 121102 (2014).

[96] M. Aguilar, D. Aisa, B. Alpat, A. Alvino, G. Ambrosi, K. Andeen, L. Arruda, N. Attig, P. Azzarello, A. Bachlechner, *et al.*, Physical Review Letters **113**, 221102 (2014).

[97] Q. Yuan, X.-J. Bi, G.-M. Chen, Y.-Q. Guo, S.-J. Lin, and X. Zhang, Astroparticle Physics **60**, 1 (2015), arXiv:1304.1482 [astro-ph.HE].

[98] H. Rishbeth, Australian Journal of Physics **11**, 550 (1958).

[99] D. K. Milne, Australian Journal of Physics **21**, 201 (1968).

[100] K. W. Weiler and N. Panagia, Astron. Astrophys. **90**, 269 (1980).

[101] F. Donato, N. Fornengo, D. Maurin, P. Salati, and R. Taillet, Phys. Rev. D **69**, 063501 (2004), astro-ph/0306207.

[102] D. Maurin, F. Donato, R. Taillet, and P. Salati, Astrophys. J. **555**, 585 (2001), astro-ph/0101231.

[103] I. Sushch and B. Hnatyk, Astron. Astrophys. **561**, A139 (2014), arXiv:1312.0777.

[104] I. Sushch *et al.*, Astron. Astrophys. **525**, A154 (2011), arXiv:1011.1177.

[105] R. L. White and K. S. Long, Astrophys. J. **373**, 543 (1991).

[106] K. S. Dwarakanath, Journal of Astrophysics and Astronomy **12**, 199 (1991).

[107] E. M. Berkhuijsen, C. G. T. Haslam, and C. J. Salter, Astron. Astrophys. **14**, 252 (1971).

[108] E. M. Berkhuijsen, Astron. Astrophys. **24**, 143 (1973).

[109] A. R. Duncan, R. T. Stewart, R. F. Haynes, and K. L. Jones, Mon. Not. Roy. Astron. Soc. **287**, 722 (1997).

[110] M. I. Large, M. J. S. Quigley, and C. G. T. Haslam, Mon. Not. Roy. Astron. Soc. **124**, 405 (1962).

[111] E. M. Berkhuijsen, Astron. Astrophys. **14**, 359 (1971).

[112] A. N. Bunner, P. L. Coleman, W. L. Kraushaar, and D. McCammon, Astrophys. J. Lett. **172**, L67 (1972).

[113] Y. Sofue, K. Hamajima, and M. Fujimoto, Publications of the Astronomical Society of Japan **26**, 399 (1974).

[114] R. J. Borken and D.-A. C. Iwan, Astrophys. J. **218**, 511 (1977).

[115] R. S. Roger, C. H. Costain, T. L. Landecker, and C. M. Swerdlyk,

Astronomy and Astrophysics Supplement Series **137**, 7 (1999), astro-ph/9902213.

[116] A. E. Guzmán, J. May, H. Alvarez, and K. Maeda, Astron. Astrophys. **525**, A138 (2011), arXiv:1011.4298 [astro-ph.GA].

[117] P. Reich and W. Reich, Astronomy and Astrophysics Supplement Series **74**, 7 (1988).

[118] D.   Borla   Tridon,   International Cosmic Ray Conference **6**, 47 (2011), arXiv:1110.4008 [astro-ph.HE].

[119] C. B. Markwardt and H. B. Ögelman, Astrophys. J. Lett. **480**, L13 (1997).

[120] V. Mangano, E. Massaro, F. Bocchino, T. Mineo,   and G. Cusumano, Astron. Astrophys. **436**, 917 (2005), astro-ph/0503261.

[121] A. Abramowski *et al.*, Astron. Astrophys. **548**, A38 (2012), arXiv:1210.1359 [astro-ph.HE].

[122] A. A. Abdo *et al.*, Astrophys. J. **713**, 146 (2010), arXiv:1002.4383 [astro-ph.HE].

[123] M.-H. Grondin, R. W. Romani, M. Lemoine-Goumard, L. Guillemot, A. K. Harding, and T. Reposeur, Astrophys. J. **774**, 110 (2013), arXiv:1307.5480 [astro-ph.HE].

[124] O. C. de Jager, P. O. Slane, and S. LaMassa, Astrophys. J. Lett. **689**, L125 (2008), arXiv:0810.1668.

[125] J. A. Hinton, S. Funk, R. D. Parsons, and S. Ohm, Astrophys. J. Lett. **743**, L7 (2011), arXiv:1111.2036 [astro-ph.HE].

[126] J. M. Blondin, R. A. Chevalier, and D. M. Frierson, Astrophys. J. **563**, 806 (2001), astro-ph/0107076.

[127] A. D. Erlykin and A. W. Wolfendale, Journal of Physics G Nuclear Physics **28**, 359 (2002).

[128] E. A. Dorfi, Astrophys. Space Sci. **272**, 227 (2000).

[129] S.-H. Lee, P. O. Slane, D. C. Ellison, S. Nagataki,   and D. J. Patnaude, Astrophys. J. **767**, 20 (2013), arXiv:1302.4645 [astro-ph.HE].

[130] A. Bamba, R. Yamazaki,   and J. S. Hiraga, Astrophys. J. **632**, 294 (2005), astro-ph/0506331.

[131] E. G. Berezhko, G. Pühlhofer, and H. J. Völk, Astron. Astrophys. **505**, 641 (2009), arXiv:0906.5158 [astro-ph.HE].

[132] H. Uchida, H. Tsunemi, S. Katsuda, and M. Kimura, Astrophys. J. **688**, 1102-1111 (2008), arXiv:0809.0594.

[133] D. Leahy and M. Hassan, Astrophys. J. **764**, 55 (2013).

[134] S. Manconi, M. Di Mauro,   and F. Donato, ArXiv e-prints   (2016),

arXiv:1611.06237 [astro-ph.HE].